Check for updates

GCB Bioenergy

WILEY

Global Change Biology Bioenergy
BIOPRODUCTS FOR A SUSTAINABLE BIOECONOMY

RESEARCH ARTICLE OPEN ACCESS

Biodiesel Production From Canola Oil by Titanium Dioxide-Photocatalysed Transesterification

Rosilene A. Welter[1,2] | Harrson Santana[1] | Lucimara G. de la Torre[1] | Osvaldir Pereira Taranto[1] | Michael Oelgemöller[2,3]

[1]School of Chemical Engineering, University of Campinas, Campinas, Brazil | [2]College of Science and Engineering, James Cook University, Townsville, Queensland, Australia | [3]Faculty of Chemistry and Biology, Hochschule Fresenius gGmbH—University of Applied Sciences, Idstein, Germany

Correspondence: Rosilene A. Welter (rosilene.weltergabas@jcu.edu.au)

Received: 24 November 2025 | **Revised:** 3 March 2026 | **Accepted:** 13 March 2026

Keywords: biodiesel | biofuels | canola oil | photocatalysis | phototransesterification | renewable fuels | thermodynamic properties | titanium dioxide

ABSTRACT

Fatty acid esters were produced by phototransesterification of canola oil using TiO_2 as a photocatalyst and employing either UVA or sunlight as radiation sources. Conversions of approximately 73% (±1.41) and 19% to fatty acid methyl esters (FAME) were achieved with methanol (1 TGL [triglyceride] mol:55 MeOH mol, 20% TiO_2 $w_{catalyst}/w_{TGL}$, 65°C, 4 h). In contrast, ethanol resulted in a lower conversion rate of 38%. Conventional thermal methods employing acid and alkali catalysts were employed to compare their corresponding FAME contents to those generated through photocatalysis. The kinetic curves were established for temperature ranges of 25°C–65°C. This study evaluated six kinetic mathematical models, among which the second forward/fourth backward model exhibited the greatest accuracy (R^2 of 0.996). This indicates that a homogeneous system model can be applied to a heterogeneous process, given that the mass transfer to the active sites of the solid catalyst is not the rate-limiting factor. The thermodynamic data ($\Delta G_{328.15K} = 29.98$ kJ/mol, $\Delta G_{338.15K} = -6.88$ kJ/mol, $\Delta H = 83.00$ kJ/mol and $\Delta S = 0.27$ kJ/mol K) suggest that this endothermic reaction requires temperatures of approximately 65°C to reach substantial conversion rates. These findings support the development of sustainable, low-waste biodiesel production pathways aligned with global decarbonisation goals.

1 | Introduction

Power generation and transportation primarily rely on fossil fuels as their main energy source. However, the growing demand for energy has led to the depletion of natural oil reserves. Furthermore, it contributes to an increase in carbon dioxide emissions, which contradicts the global 2030 goal of reducing greenhouse gas emissions by approximately 50%. In the area of sustainable energy, biodiesel has emerged as a potential replacement for traditional fossil fuels. It is compatible with current diesel engines without significant alterations, an eco-friendly option for commercial, public and heavy-duty transport, and also suitable for electricity supply (Nagrale 2024). As a result, its production has grown significantly due to its versatility and wide-ranging applications. From 2005 to 2020, there was an eightfold increase, with annual output reaching 46 billion litres (Ogunkunle and Ahmed 2019). Furthermore, a projected increase to 59 billion litres is anticipated by 2030, with the aviation and shipping sectors accounting for 75% of the demand (Pandey 2024).

Biodiesel offers significant environmental advantages as it releases 86% fewer greenhouse gases compared to conventional fuels (Voegele 2020). It is furthermore degraded four times more rapidly than petrofuels (Voegele 2020) and is derived from renewable sources (e.g., vegetable oils, waste cooking oil [WCO] and animal fats—according to ASTM D6751-15; ASTM International 2015). Canola oil, accounting for 68% of the global biodiesel feedstock, is amongst the most widely produced and consumed vegetable oils worldwide (Kim et al. 2018). Despite the obvious competition with the food industry, it is crucial to explore novel methods for biodiesel production from this

This is an open access article under the terms of the Creative Commons Attribution License, which permits use, distribution and reproduction in any medium, provided the original work is properly cited.

© 2026 The Author(s). *GCB Bioenergy* published by John Wiley & Sons Ltd.

resource as it remains an important feedstock of biodiesel production. Furthermore, investigating processes using canola oil sheds light on potential new approaches for biodiesel production from related fatty acid sources.

Biodiesel is a blend of long-chain fatty acid alkyl esters (FAAE) primarily produced through esterification and/or transesterification. Transesterification, the most common reaction, occurs between triglycerides (TGL) and alcohols in the presence of a catalyst such as strong acids or alkalis, producing FAAE and glycerol. However, these conventional homogeneous approaches require extensive separation and purification steps resulting in the production of large amounts of waste (Berrebi et al. 1994). These issues may be circumvented by solid eco-friendly catalysts such as metal oxides, enzymes, zeolites and alumina (Alsharifi et al. 2017; Arzamendi et al. 2007; Calero et al. 2014; Corro et al. 2013; dos Passos et al. 2024; Omar and Amin 2011; Welter, Santana, et al. 2022; Yang et al. 2024). Heterogeneous catalysts typically offer advantages such as easy separation and regeneration, exhibit improved safety and practicality in handling, and tend to be less corrosive in nature (Chouhan and Sarma 2011; De and Boxi 2020; Granados et al. 2007; Ma and Hanna 1999). Since temperature plays a crucial role in enhancing yields, some researchers have explored different methods to increase the temperature of the solid catalyst surface, where the reactions start, instead of the entire system. Technologies such as microwave and laser have been employed to boost the reaction rate by this approach (Yue et al. 2024).

One promising alternative technology is the use of photoactivated solid catalysts. Examples are titanium dioxide (TiO_2, UVA), and Ni/Si/MgO (Visible), SnS_2/ZIF (Visible) (Gadore et al. 2025; Islam et al. 2025; Welter, Santana, et al. 2022). TiO_2 is non-toxic, chemically stable, easy to handle, and recyclable (Carp et al. 2004). While heterogeneous photocatalysis has been extensively investigated for the degradation of organic contaminants such as dyes, pesticides and pharmaceuticals (Kanakaraju et al. 2014; Konstantinou and Albanis 2003; Rajeshwar et al. 2008), its application in organic synthesis has received comparatively less attention (Hoffmann 2015). However, photocatalysis has recently been evaluated as a potential alternative for biodiesel production through esterification and transesterification. For example, oleic acid and methanol photoesterification was achieved using TiO_2 and UVA-irradiation, resulting in 98% conversion (Welter, Santana, et al. 2022). TiO_2 nanotubes and sunlight irradiation gave 91% conversion for waste cooking oil (WCO) transesterification (Khaligh et al. 2021). Likewise, TiO_2/g-C_3N_4 under sunlight irradiation resulted in a 90% conversion for TGL from WCO (Khan, Farah, et al. 2021). The attractive advantages of photocatalysis are its sustainable operation conditions in mild temperatures and pH ranges, yielding higher-purity products that can be recovered easily, and the simple reuse of the catalyst. TiO_2-photocatalyis using natural sunlight has also been applied to the manufacturing of commodity chemicals and to water treatment (Bahnemann 2004; Oelgemöller 2016). Although the focus of photocatalysis has turned towards biodiesel production via esterification and transesterification, it offers esterification and transesterification pathways to other products such as amino acids (Tomiya et al. 2024), acetic acid esters (Özyiğit et al. 2024), and biodiesel from WCO using porphyrin as a photocatalyst (Mataghare et al. 2024). Despite their importance for developing cost-efficient and scalable processes, limited research has thus far explored the kinetic and thermodynamic aspects of photocatalysis.

The present study evaluated photoactivation of TiO_2 with UVA or sunlight for canola oil transesterification with methanol or ethanol. The aim was to provide essential experimental data to achieve the best operational conditions, establish a reliable process protocol, and determine kinetic and thermodynamic properties.

2 | Materials and Methods

2.1 | Materials

Reagents and solvents were obtained from the following suppliers: canola oil (Woolworths), TiO_2 (P25: Aeroxide, Evonik), methanol (HPLC grade, Fisher Chemical), chloroform D (99.8% atom D, $CDCl_3$, Aldrich), dichloromethane (DCM, AR, 99.5%, Univar), sulphuric acid (AR, Univar), potassium hydroxide pellets (KOH, Univar), acetone (AR, 99.5%, Chemsupply), diethyl ether (AR, 99.5%, Univar), ethyl acetate (AR, 99.5%, Univar), ethanol (AR, 99.5%, Univar), 0.02 N potassium hydroxide in aqueous solution ($KOH_{aqueous}$, ±0.5%, Ace Chemical Company), sodium bicarbonate ($NaHCO_3$, AR, Univar), and anhydrous sodium sulphate (Na_2SO_4, AR, Univar), 1-oleoyl-rac-glycerol (Standard solution, Sigma), dioleoylglycerol (Standard solution, Sigma), 1,3-diolein (Standard solution, Sigma), Lipid Standard, Mono-, Di-, & Triglyceride Mix (Standard solution, Sigma), FAME mix (Standard solution, Supelco).

2.2 | Canola Oil Transesterification

Canola oil transesterification with alcohol was carried out using four different conditions: alkali-catalysis (KOH), acid-catalysis (H_2SO_4), UVA/TiO_2-photocatalysis and solar TiO_2-photocatalysis. The first two methods represent the most common thermal processes and were developed to establish a comparison between the biodiesels obtained thermally with that from photocatalysis. An additional experiment was conducted using acid catalysis but with a shorter reaction time in order to examine the presence of possible intermediates, that is monoglycerol (MG) and diglycerol (DG). The use of acidic catalyst was chosen over the alkaline one because the acid-catalysed process is slower, facilitating the detection of intermediates, which was the primary objective of this experiment.

2.2.1 | Alkali Catalysis

Anhydrous methanol (150 mL), canola oil (15 g) and KOH (1.5 g) were added to a round-bottom flask (250 mL). The mixture was stirred rapidly with a magnetic stirrer at 90°C for 2 h. The mixture was then allowed to settle for 24 h at room temperature. The product was purified using the following steps: (1) 600 mL of water was added; (2) the liquid alcoholic phase was removed by rotary evaporation at 40°C (170 mbar for 60 min, 72 mbar for 60 min, and 30 mbar for 60 min); (3) for three consecutive times, 150 mL of ethyl acetate was added

17571707, 2026, 6, Downloaded from https://onlinelibrary.wiley.com/doi/10.1111/gcbb.70113 by James Cook University, Wiley Online Library on [10/11/2026]. See the Terms and Conditions (https://onlinelibrary.wiley.com/terms-and-conditions) on Wiley Online Library for rules of use; OA articles are governed by the applicable Creative Commons License

and mixed gently, allowed to settle for 1 h in a separatory funnel, and the organic layer was separated; (4) 150 mL of diluted HCl 0.5% (v/v) solution was added, mixed, and the mixture was separated into two phases; (5) 150 mL of a saturated aqueous NaCl solution was added, mixed, and allowed to separate into phases; (6) the organic layer was separated and dried with anhydrous Na_2SO_4 for approximately 5 min; (7) the reaction mixture was filtered using a syringe filter (Hydraflon 0.22 μm, 35 mm); (8) the crude product was rotary-evaporated at 40°C to remove the solvent and any volatiles (170 mbar for 30 min, 72 mbar for 30 min, and 30 mbar for 60 min); (9) the samples were stored in glass vials at room temperature for further characterisation.

2.2.2 | Acid Catalysis

Test 1 (complete conversion): anhydrous methanol (150 mL), canola oil (15 g) and H_2SO_4 (1.5 g) were added to a round-bottom flask (250 mL), stirred rapidly with a magnetic stirrer at 90°C for 5 h, and left to stand for 24 h at room temperature. The product was purified following the steps described above for alkali catalysis but using 150 mL of a dilute $NaHCO_3$ solution in step (4). Test 2 (incomplete conversion): the same steps mentioned above (Section 2.2.1) were used; however, the reagents were mixed for 1 h instead of 5 h, and purification was performed immediately.

2.2.3 | UVA/TiO_2-Photocatalysis

The catalyst pretreatment and operational conditions were adopted from the optimised photoesterification process developed by Welter and co-workers (Welter, Santana, et al. 2022; Welter et al. 2026). The light and water flow, and reaction heating (water-bath) were turned on 30 min before each phototransesterification experiment. TiO_2 was added to methanol and mixed at the respective phototransesterification test temperature (25°C–65°C, Table S.1). After stirring for 30 min, TiO_2 and MeOH (20% TiO_2 $w_{catalyst}/w_{TGL}$, and 1 TGL mol:55 methanol mol, total volume of reactional medium: 100 mL) were loaded into the reactor (Figure 1a) filled with canola oil. The double jacketed two-necked round-bottom flask vessel (500 mL capacity) was manufactured using Pyrex glass (cut-off wavelength ≤ 290 nm). Irradiation was conducted in a Rayonet RPR-200 photochemical reactor (Southern New England Ultraviolet Company) equipped with 16 F8T5/BL fluorescent tubes (Ushio, 8 W Black Light UVA T-5 G5 Base). The oil, methanol, and TiO_2 were mixed vigorously by magnetic stirring. During the kinetic studies, samples (< 3 mL each) were withdrawn at set reaction times (15, 30, 45, 60, 120, 180, and 240 min). The reactions were stopped after presumably reaching equilibrium (240 min) and treated using the following steps: (1) filtered through a syringe filter (Hydraflon 0.22 μm, 35 mm); (2) rota-evaporated at 40°C to remove water and alcohol (170 mbar for 15 min, 72 mbar for 30 min, and 30 mbar for 30 min); (3) left to stand for 20 h to allow for glycerine separation; (4) stored in glass vials at room temperature; (5) conversion determined by ^{1}H-NMR as described in Section 2.3.1; (6) the final sample (240 min) was further characterised (Section 2.3.2). Following the development of all tests, the most successful one was conducted three times to determine the experimental margin of error. Five blank tests were performed by keeping the operational conditions constant (65°C, 1 TGL mol:55 MeOH mol, and 20% TiO_2 $w_{catalyst}/w_{TGL}$): Blank 1 (absence of catalyst); Blank 2 (absence of light with the reaction vessel wrapped in aluminium foil); Blank 3 (absence of catalyst and light with the reaction vessel wrapped in aluminium foil); Blank 4 (absence of stirring); Blank 5 (absence of catalyst pretreatment). FAEE was also produced, applying the best operational conditions obtained previously for FAME, but using ethanol instead of methanol.

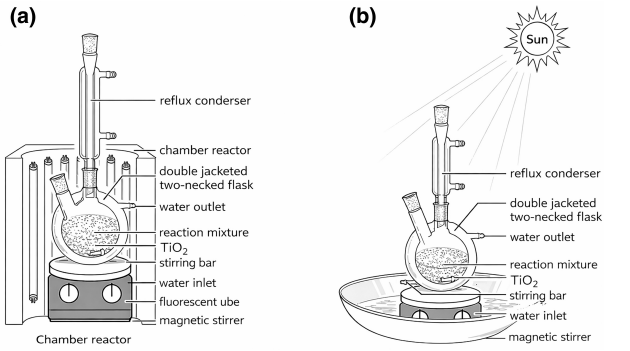


FIGURE 1 | Schematic representation of the phototransesterification reactors used in this study: (a) UVA-driven reactor equipped with fluorescent lamps, and (b) solar-driven reactor under natural sunlight. Both systems consist of a double-jacketed two-necked flask connected to a reflux condenser, with continuous stirring and temperature control via water circulation. The reaction mixture contains canola oil, alcohol, and TiO_2 photocatalyst.

2.2.4 | Concentrated Solar/TiO_2-Photocatalysis

Considering the best operational conditions achieved with artificial UVA light (Section 2.2.3), the transesterification of canola oil was examined using natural sunlight (Figure 1b) instead of UVA light (Figure 1a). The apparatus consists in a spherical stainless-steel dish (S21400, inner diameter of 44 cm, focal length of 16.13 cm) below the double-jacketed round-bottom reactor. The reaction was conducted on the ground outside the Molecular Genetic Laboratory Building on the James Cook University campus in Townsville (latitude—19°33′ S, longitude 146°46′ E, elevation 37.2 m above sea level) for 360 min, from 9:30 AM to 3:30 PM, the period with the highest radiation. The sunlight irradiation measurements for Townsville were obtained from ARPANSA (2022) (Section S2.2).

2.3 | TiO_2 Catalyst

2.3.1 | Recovery, Reactivation and Reuse

After each photochemical experiment, the catalyst was recovered and treated using the following steps: (1) filtered through a filter paper (Grade: MS 2 185 mm, MicroScience); (2) washed with acetone by mixing vigorously with magnetic stirring (500 rpm); (3) settled for 20 h followed by decantation; (4) dried at 100°C for 24 h; and (5) crushed. These steps represent the first stage of the recovery process (1 RP). This process was repeated three times (3 RP) to complete one reactivation cycle (1 C). The samples were stored in plastic vials at room temperature. The efficiency and reusability of the recovered TiO_2 were

17571707, 2026, 6, Downloaded from https://onlinelibrary.wiley.com/doi/10.1111/gcbb.70113 by James Cook University, Wiley Online Library on [10/11/2026]. See the Terms and Conditions (https://onlinelibrary.wiley.com/terms-and-conditions) on Wiley Online Library for rules of use; OA articles are governed by the applicable Creative Commons License

evaluated using the characterisation techniques described in Section 2.4.2 and by conducting five subsequent photoreaction tests (1C–5C).

2.3.2 | Characterisation

TiO_2 was characterised before (pure), after use (0RP), after reactivation (1C), and after reuse (2C–5C) using the following analyses. Thermogravimetric analysis (TGA) and differential scanning calorimetry (DSC) (5°C/min, room temperature to 600°C, SDT650 equipment) were performed to determine the presence of organic material impregnated on the catalyst material. The data were subsequently analysed using the Trios software (T.A. Instruments). Two samples were analysed in triplicate: one with the highest content (0RP) and one with the lowest content (5C) of organic material. The particle size, pore volume and size, and total surface area were determined using N_2 physisorption (Quantachrome Instruments 2009). The surface area was determined using the BET model (Equation 1), correlating the surface coverage (θ), BET constant (c), pressure (p), and vapour pressure of the adsorptive bulk liquid phase (p_0). Pore volume and diameter were determined using the BJH model (Equation 2), which is based on the Kelvin equation and correlates p, p_0, the gas/liquid surface tension (Y), molar volume of the adsorbate (M), gas constant (R), and temperature (T). The particle size (Equation 3) was established by relating the surface area (S_{BET}) and the solid density (ρ, 4.2 g/mL for TiO_2) (Raj and Viswanathan 2009).

$$\theta = \frac{cp}{\left(1 - p/p_0\right) \cdot \left(p_0 + p(c-1)\right)} \tag{1}$$

$$\ln \frac{p}{p_0} = \frac{-2YM}{RT} \tag{2}$$

$$D = \frac{6000}{S_{BET} \cdot \rho} \tag{3}$$

Fourier transform infrared–attenuated total reflection (FTIR-ATR) spectroscopy was conducted at room temperature, over the spectral range of 400–1000 cm^{-1} (Nicolet iS 5 FTIR Spectrometer coupled with an iD7 ATR accessory, Thermo Fisher Scientific) to detect the presence of organic functional groups. The TiO_2 bandgap (E_g) was obtained by UV–Vis spectroscopy at room temperature over the spectral range of 200–1100 cm^{-1} (UV-1800, Shimadzu) using the Tauc method (Equation 4) (Arunachalam et al. 2015; Kulak and Kiiliomin 2018; Makuła et al. 2018; Tauc et al. 1966). The model correlates the absorption coefficient (α), photon energy ($h\nu$), a constant (B), and a factor (Y) that depends on the nature of the electron transition (0.5 for direct and 2.0 for indirect transition band gaps). For TiO_2, $Y = 2$ was considered (Makuła et al. 2018). The TiO_2 suspension was prepared by vigorously mixing 10^{-3} mg/L TiO_2 in methanol for 4 h.

$$(\alpha \cdot h\nu)^{1/\gamma} = B \cdot \left(h\nu - E_g\right) \tag{4}$$

The crystal structure and crystallite size were examined by powder X-ray diffraction (XRD, Siemens D5000 Diffractometer) using Cu Kα radiation ($\lambda_{XRD} = 0.154060$ nm). The mean crystallite size was obtained by analysing the prominent peak observed in the XRD pattern for anatase (25.23° 2θ) and rutile (27.43° 2θ), respectively. The Scherrer equation (Equation 5) was used to estimate the crystallite size according to Equation (7) assuming K_{XRD} equal 0.9 and λ_{XRD} equal to 1.5406 Å.

$$D_C = \frac{K_{XRD} \cdot \lambda_{XRD}}{\beta_{XRD} \cdot \cos\theta_{XRD}} \tag{5}$$

2.4 | Product Analysis

2.4.1 | Conversion

The biodiesel concentration was determined by ^{1}H-nuclear magnetic resonance (NMR) spectroscopy (*Bruker Ascend 400 MHz* Spectrometer) by comparing the integration areas of baseline-separated signals using the MestReNova software (Version 6.0.2-5476, Mestrelab Research S.L.). The FAME amount (Equation 6) was calculated by correlating the three methoxy protons (I_{ME}, approx. 3.6 ppm) with the two α-methylene protons of the oil ($I_{\alpha CH_2}$, approx. 2.3 ppm) (Borah et al. 2018; Gelbard et al. 1995). The FAEE concentration was obtained similarly (Equation 7) by correlating the glyceride CH_2 (I_{GL}) and ethoxy (I_{EE}) proton areas (I_{GL+EE}, overlapping peaks at 4.10–4.20) with the α-methylene protons area of the oil ($I_{\alpha CH_2}$, 2.3 ppm) (Jaiswal et al. 2016) (Section S3).

$$\%\,\text{FAME} = 100\,\% \cdot \frac{2 \cdot I_{ME}}{3 \cdot I_{\alpha CH_2}} \tag{6}$$

$$\%\,\text{FAEE} = 100\,\% \cdot \frac{I_{GL+EE} - I_{GL}}{I_{\alpha CH_2}} \tag{7}$$

2.4.2 | Physico-Chemical Characterisation

GC/MS analysis was employed to determine the composition of the raw material, intermediates, and products. To account for all potentially present compounds, two distinct approaches were employed. Firstly, the analysis was carried out according to the EN 14103 (European Committee for Standardization 2003) using an HP-5INNOWax capillary column (30 m × 0.25 mm × 0.25 μm) (McCurry 2012). Pure helium was used as the carrier gas (1 mL/min). The temperature programme used was 60°C for 2 min, 10°C/min to 200°C, 5°C/min to 240°C, and holding at 240°C for 7 min. Second, the analysis was carried out according to the ASTM D6584 (ASTM International 2017c) methodology using a Zebron ZB-5HT capillary column (15 m × 0.32 mm × 0.10 μm). Pure helium was employed as the carrier gas (3 mL/min). The temperature programme used was 50°C for 1 min, then to 180°C (15°C/min), to 230°C at 7°C/min, and then up to 380°C.

Additionally, ATR-FTIR spectroscopy was used to chemically analyse the oil and FAME. The acid value was determined by titration using a modified procedure as follows (Du et al. 2022; European Committee for Standardization 2003; Onu and Mbohwa 2021). The organic sample (0.05 g) was diluted in a diethyl ether/ethanol solution (2:1, 25 mL) (v/v). Two drops of thymol blue indicator were added, and the analyte was titrated using a 0.02 N KOH aqueous standard solution. The acid value (AV) was calculated as described in Equation (8), correlating the volume of the KOH solution used in the titration (S, mL), the

17571707, 2026, 6, Downloaded from https://onlinelibrary.wiley.com/doi/10.1111/gcbb.70113 by James Cook University, Wiley Online Library on [10/11/2026]. See the Terms and Conditions (https://onlinelibrary.wiley.com/terms-and-conditions) on Wiley Online Library for rules of use; OA articles are governed by the applicable Creative Commons License

TABLE 1 | Kinetic models evaluated for canola oil and methanol phototransesterification.

Assumptions	Model	Equation
Homogeneous system		
F1B1		
FR: first-order	$\frac{dx_{TGL}}{dt} = k_1 \cdot (1 - x_{TGL}) - k_{-1} \cdot x_{TGL}$	Equation 15
BR: first-order		
F1B2		
FR: pseudo-first-order	$\frac{dx_{TGL}}{dt} = k_1 \cdot (1 - x_{TGL}) - k_{-1} \cdot C_{TGL_0} \cdot x_{TGL}^2$	Equation 16
BR: second-order		
F2B2		
FR: second-order	$\frac{dx_{TGL}}{dt} = k_1 \cdot C_{TGL_0} \cdot (1 - x_{TGL})^2 - k_{-1} \cdot C_{TGL_0} \cdot x_{TGL}^2$	Equation 17
BR: second-order		
F1B3		
FR: first-order	$\frac{dx_{TGL}}{dt} = k_1 \cdot (1 - x_{TGL}) - k_{-1} \cdot C_{TGL_0}^2 \cdot x_{TGL}^3$	Equation 18
BR: third-order		
F2B4		
FR: second-order	$\frac{dx_{TGL}}{dt} = k_1 \cdot C_{TGL_0} \cdot (1 - x_{TGL})^2 - k_{-1} \cdot C_{TGL_0}^3 \cdot x_{TGL}^4$	Equation 19
BR: fourth-order		
Heterogeneous system		
L–H kinetic model[a]		
FR: first-order	$\frac{dx_{TGL}}{dt} = k_1 \cdot \frac{K_2' \cdot x_{TGL}}{1 + K_2' \cdot C_{TGL_0} \cdot x_{TGL}} - k_{-1} \cdot \frac{K_1' \cdot (1 - x_{TGL})}{1 + K_1' \cdot C_{TGL_0} \cdot (1 - x_{TGL})}$	Equation 20
BR: first-order		

[a]L-H model details are shown in Supporiting Information - Section S7. FR: Forward reaction. BR: Backward reaction.

volume of the KOH used in the blank titration (b, mL), the normality of KOH (N), and the sample mass (W, g):

$$AV = \frac{(Sb) \cdot N \cdot 56.1}{W} \tag{8}$$

TGA/DSC (SDT650 equipment) was used to determine the maximum combustion rate $[(dM/dT)_{max}]$ (Lai et al. 2014; Wnorowska et al. 2021), mean combustion rate $[(dM/dT)_{mean}]$ (Lai et al. 2014), burnout temperature (T_e) (Lu and Chen 2015; Wnorowska et al. 2021) and ignition temperature (T_i) (Khan, Farah, et al. 2021; Lu and Chen 2015; Wnorowska et al. 2021). Air and nitrogen were used for operations. The temperature was increased from room temperature to 600°C at a heating rate of 10°C/min. The data were analysed using the Trios software (T.A. Instruments) and OriginPro 2021 (Learning Edition, OriginLab Corporation). The activation energy (E_a) was estimated using the Arrhenius model (Equation 9) and expressed analytically according to the Coats–Redfern method (Equation 10) by correlating the heating rate (β), gas constant (R, 8.314 J/mol K), T (K) and mass loss according to the α parameter (Equation 11), where W_o, W_{TI} and W_f are the initial weight, weight at $T_{ignition}$ and final weight, respectively (Cai and Bi 2008; Kipcak et al. 2015; Yao et al. 2008).

$$\ln(k) = -\frac{\Delta E}{R \cdot T} + \ln(A) \tag{9}$$

$$\log\left[\frac{-\log(1-\alpha)}{T^2}\right] = \log\frac{A \cdot R}{\beta \cdot E_a}\left[1 - \frac{2 \cdot R \cdot T}{E_a}\right] - \frac{E_a}{2.303 \cdot R \cdot T} \tag{10}$$

$$\alpha = \frac{W_O - W_{T_I}}{W_O - W_f} \tag{11}$$

3 | Kinetic and Thermodynamic Properties

Five kinetics experiments were conducted for canola oil and methanol phototransesterification with TiO_2 at different temperatures (range: 25°C–65°C; operational conditions described in Section 2.2.3). Six kinetic models, and the proposed reaction conditions, were evaluated (Table 1). Despite the non-homogeneous nature of the system, a first-order reversible model was found to be suitable for sunflower oil transesterification using ZnO as the catalyst (Khezrianjoo and Revanasiddappa 2012). The fundamental key involves treating the system as homogeneous with complete miscibility between the reactants, and neglecting mass transfer effects. In line with this approach, five distinct models were evaluated, with varying orders of forward and backward reactions. The sixth model, Langmuir–Hinshelwood (L–H), considered a system with complete miscibility among reagents and a heterogeneous catalyst

17571707, 2026, 6, Downloaded from https://onlinelibrary.wiley.com/doi/10.1111/gcbb.70113 by James Cook University, Wiley Online Library on [10/11/2026]. See the Terms and Conditions (https://onlinelibrary.wiley.com/terms-and-conditions) on Wiley Online Library for rules of use; OA articles are governed by the applicable Creative Commons License

with homogeneous active sites. This model was satisfactory applied for oleic acid and waste cooking oil in the presence of methanol and ethanol by photoesterification using a heterogeneous catalyst (Welter et al. 2026). It is frequently employed in photocatalytic processes involving catalysts within the nanoscale range (Brahim et al. 2021; Chaemchuen et al. 2020; Choo 2018; Ezzati 2018; Kar et al. 2012; Karan et al. 2020; Khezrianjoo and Revanasiddappa 2012).

Mathematical modelling was performed using the MATLAB software package, and the results were evaluated statistically (R^2, F-test, SD, β, t-value, and p-value) using the Statistica 7.0 software (StatSoft Inc.). Subsequently, the kinetic parameters (k_1, k_{-1}, $E_{a,}$ and A), which are fundamental to understanding the reaction performance over time, were obtained. The activation energy (ΔE_a) and frequency factor (A) were determined using the Arrhenius model (Equation 9). Likewise, the equilibrium constant (K_{eq}) and the thermodynamic properties (ΔH, ΔS, and ΔG) were determined. The enthalpy (ΔH) and entropy (ΔS) were determined using the Van't Hoff model (Equation 12). The Gibbs free energy variation (ΔG), dependent on temperature, was determined using two different models. Firstly, by correlating temperature and the equilibrium constant (K_{eq}) (Equation 13), and secondly by correlating enthalpy, entropy, and temperature (Equation 14). Both results were compared and evaluated statistically (p-value and t-value).

$$\ln(K) = -\frac{\Delta H}{R \cdot T} + \frac{\Delta S}{R} \tag{12}$$

$$\Delta G = -R \cdot T \cdot \ln(K_{eq}) \tag{13}$$

$$\Delta G = \Delta H - T \cdot \Delta S \tag{14}$$

4 | Results and Discussion

This section presents the analyses of biodiesel production via photocatalysis. Firstly, the results regarding the catalyst (TiO_2) physico-chemical characterisation is shown in Section 4.1. Subsequently, Section 4.2 examines the photoesterification and transesterification reactions focusing on process efficiency due to the operation conditions. The following Section 4.3 emphasises the product (FAME and FAEE) characterisation and comparison with products obtained by thermal routes (acid and alkali). Section 4.4 explores the significance of intermediates in the reaction, such as MG and DG. Finally, Section 4.6 delivers

TABLE 2 | Solid catalyst reuse for FAME production by transesterification.

Catalyst	Feedstock	FAME[a] (%)	# cycles	FAME[b] (%)	Decrease (%)	References
TiO_2 + UVA	Canola oil	73	5	36	37	This study
Ce/AC_{cs}-S	Chicken fat oil	93	5	90	3	Shobhana-Gnanaserkhar et al. (2020)
HSiW/Al	Canola oil	39	4	38	1	Gaurav et al. (2019)
TiO_2/$PrSO_3H$	Virgin oil + oleic acid	98	6	21	77	Gardy et al. (2017)

[a]Decrease between first and last cycle.
[b]Conversion determined for the final cycle.

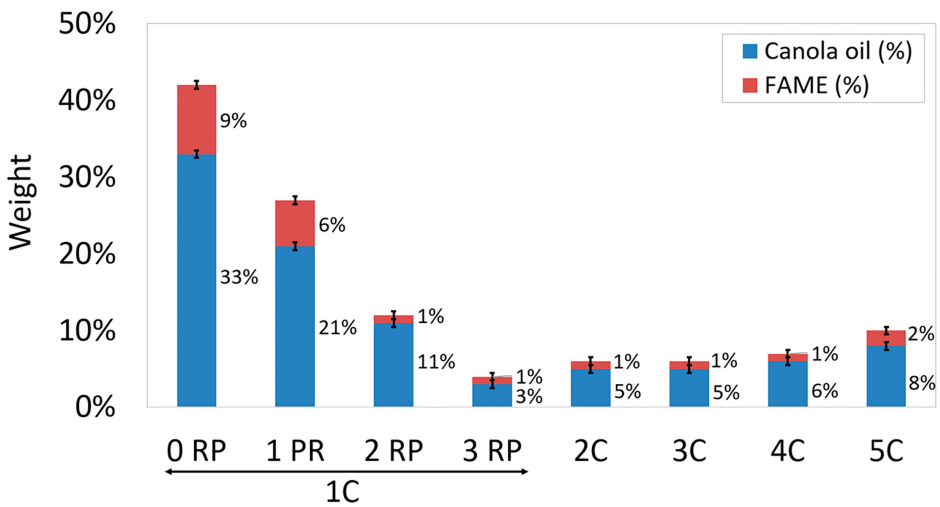


FIGURE 2 | Organic material remaining on TiO_2 after transesterification of canola oil with methanol under different reaction conditions. Blue bars represent FAME and red hatched bars represent residual canola oil. RP denotes photocatalytic runs and C denotes washing cycle. The numbers above each bar indicate total organic material, while individual values correspond to FAME and oil fractions. Asterisks (*) indicate FAME ≤1%. Error bars represent standard deviation.

17571707, 2026, 6, Downloaded from https://onlinelibrary.wiley.com/doi/10.1111/gcbb.70113 by James Cook University, Wiley Online Library on [10/11/2026]. See the Terms and Conditions (https://onlinelibrary.wiley.com/terms-and-conditions) on Wiley Online Library for rules of use; OA articles are governed by the applicable Creative Commons License

the kinetic data and thermodynamic properties obtained by both experimental results and mathematical modelling approaches.

4.1 | TiO_2 Characterisation

TiO_2 was characterised qualitatively and quantitatively at different stages of the phototransesterification process, and the most important results are highlighted in Table 2 and Figure 2. Firstly, the presence of organic material adhered onto the catalyst was explored. FTIR-ATR spectroscopy (Figure S.16) confirmed that canola oil and biodiesel were present within the catalyst material. TGA/DSC after the photoreactions (Figure 3, Section S4) indicated that substantial amounts of organic material (42% w/w) were present within the TiO_2 material after the reaction (0RP). When compared to a similar process utilising oleic acid photoesterification instead (Yang et al. 2024), the catalyst retained only 27% (w/w) organic material. The variation may be due to the miscibility of oleic acid in methanol, which enhances the mass transfer between the phases. Moreover, in both cases the primary components within the catalyst were the feedstocks (canola oil and oleic acid). This suggests that the pores were likely saturated at the beginning of the reaction when these substances were present in higher concentrations. As time progressed, oleic acid molecules, being smaller in size, could potentially move across phases, whereas the TGL chains were presumably trapped within the catalyst. The DTA results (Figure 4) revealed two main degradation areas. The first corresponding to FAME (110°C–280°C, Peaks 1.a and 1.b) and the second to canola oil (280°C–500°C, peaks 2.a and 2.b). Within both areas, peak splitting can be observed. This behaviour is due to the organic material distribution within the TiO_2 surface and inside its pores and small channels. External organic material is removed faster (1st peak), whereas organic material inside the pores is removed more slowly (2nd peak).

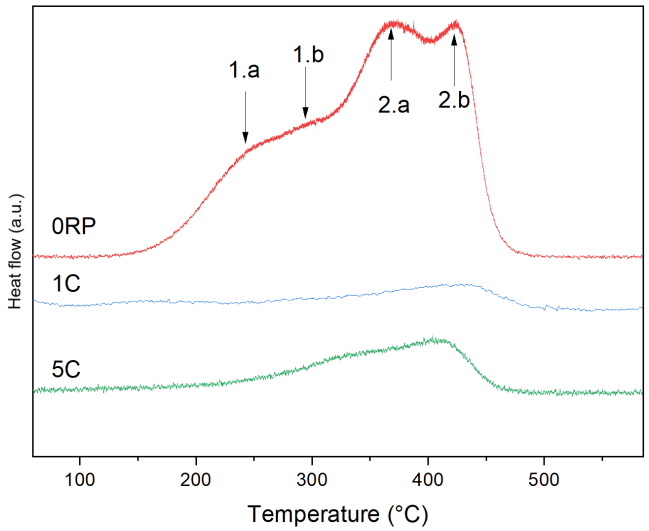


FIGURE 3 | Differential thermal analysis (DTA) curves of TiO_2 used in canola oil transesterification with methanol, measured from room temperature to 600°C. Samples correspond to the catalyst after use without reactivation (0RP), after use followed by the washing cycle (1C), and after use with reactivation over five cycles (5C). Peaks labelled 1a and 1b are associated with FAME-related thermal decomposition, while peaks 2a and 2b correspond to residual canola oil species. Differences in peak intensity indicate variations in organic material accumulation on the catalyst surface.

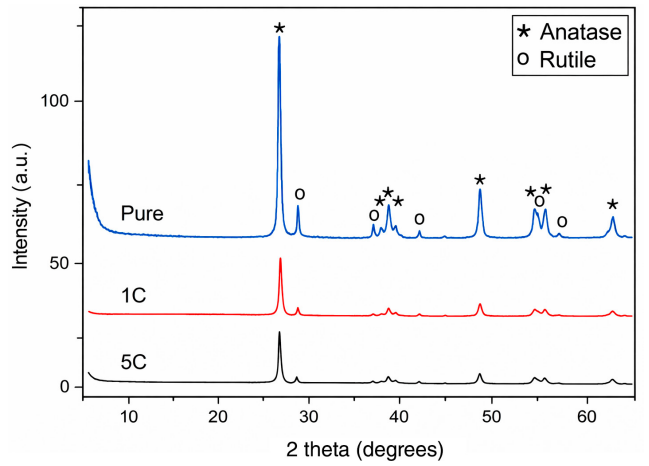


FIGURE 4 | X-ray diffraction (XRD) patterns of TiO_2 in its pristine form (Pure), after one cycle with washing (1C), and after five cycles with catalyst recovery (5C). Diffraction peaks corresponding to anatase (*) and rutile (○) phases are indicated. The patterns show the preservation of the crystalline structure of TiO_2 after repeated use and recovery processes.

The regeneration process indicates that it is possible to remove both reactants and products for reuse. The complete recovery and washing process (3 RP) effectively removed 97% (±0.69 w/w) of the organic material (18% ± 0.69 w/w) of FAME and 82% (±0.69) w/w of canola oil. After five complete photocatalytic cycles and subsequent reactivation (5C), 10% (±0.69) w/w of organic material remained on the TiO_2 (2% ± 0.69 w/w of FAME and 8% ± 0.69 w/w of canola oil). Comparison of the organic material retained in tests 1C and 5C confirmed that the reagent (canola oil) preferentially remained in the catalyst's structure. This difference in retention impacted negatively on the catalyst performance during subsequent reuse.

The recovery process of this work is a simple three-step sequence, including filtration, solvent washing and moderate-temperature drying, as described in Section 2.4.1, Recovery, reactivation and reuse. There were no high-temperature calcinations or aggressive chemical treatments necessary. Thus, the related energy consumption must also be much lower than with conventional catalyst regeneration methods using heat treatment at higher temperatures, usually above 400°C.

The washing step involves relatively small volumes of solvent, in contrast to huge amounts of water that are usually demanded by conventional alkali-catalysed biodiesel purification. In classical alkali-catalysed systems, the amount of water required for washing out soaps and unused catalyst is very high, leading to high wastewater volumes. In contrast, in the photocatalytic case, the solid catalyst can be filtered off and washed with solvent in a straightforward pathway.

The organic removed material appears largely as adsorbed triglycerides, partial glycerides and FAME residues. These compounds are primary reactants and not end products, as no parallel reaction or significant impurity by-products were found. Thus, in an industrial procedure, this fraction can

17571707, 2026, 6, Downloaded from https://onlinelibrary.wiley.com/doi/10.1111/gcbb.70113 by James Cook University, Wiley Online Library on [10/11/2026]. See the Terms and Conditions (https://onlinelibrary.wiley.com/terms-and-conditions) on Wiley Online Library for rules of use; OA articles are governed by the applicable Creative Commons License

simply be recycled to the reactor without further treatment as waste.

In addition, the solvent used in the washing step can be easily recovered by a simple single-step distillation. The temperature needed is relatively mild, as the boiling point of acetone is far below that of most organic components in the mix; therefore, ensuring a very energy-efficient separation. Therefore, both the solvent and the organic residue can be reused in the process, leading to a reduction of the environmental and economic footprint of the catalyst recovery step.

TABLE 3 | TiO_2 characterisation.

	Pure	0RP[a]	1C[a]	5C[a]
Canola oil content (% w/w)	—	33	1	8
FAME (% w/w)	—	9	3	2
Pore volume (cm^3/g)	0.74	—	0.52	0.45
Pore diameter (nm)	3.52	—	3.52	3.06
Surface area (m^2/g)	51.85[b]	—	42.78	38.23
Particle size (nm)	27.55	—	33.37	37.37
Crystallite size (nm)	22.23	—	22.87	22.82
Anatase (%)	91	—	92	90
Rutile (%)	9	—	8	10
Bandgap[c] (eV)	3.22[d]	4.49	3.28	3.56

[a]TiO_2 after phototransesterification reaction (0RP), 1C: after 1 cycle of phototransesterification and 3RP; 5C: after 5 cycles of phototransesterification and 3RP.
[b]Surface area standard value according to the manufacturer: 35–65 mg^2/g (Mostafa and El-Gendy 2017).
[c]Error: ±0.02.
[d]Bandgap of pure TiO_2 (P25, Evonik) standard value according to the literature: 3.18 eV (Nicolau et al. 2018).

N_2 physisorption and XRD analyses were performed on the pure catalyst, after use (0RP), after the recovery and washing process (1C) and after five uses (5C). Sample 0RP could not be analysed due to the high organic load present, as naturally expected in the absence of any washing process. The analysis of nitrogen physisorption (pore volume and diameter, surface area, and particle size) reveals catalyst poisoning through the presence of organic material, hence obstructing the pores. Moreover, the surface area, pore volume, and diameter decrease, while particle size increases. This finding indicates particle aggregation, causing the obstruction of the light reaching the catalyst and a reduced number of active sites available, thereby reducing the effectiveness of the photocatalyst.

The crystal properties were determined by X-ray diffraction. The crystallite size was found to have an average of 22.64 ± 0.29 nm (Table 3 and Figure 5), consisting of 91% of anatase and 9% of rutile. This composition remained unchanged after the subsequent photoreactions. The peak intensities changed with each reuse cycle due to the presence of organic material and reduced access to the core. This variance directly affected the bandgap of the catalyst. Before use (pure TiO_2) the bandgap agreed with the literature (3.2 eV). Following the reaction, the bandgap exhibited a significant increase to 4.49 eV without undergoing a reactivation via washing. Nevertheless, after a single reactivation process (1C), the bandgap increased by merely 2%, whilst five reactivation cycles (5C) resulted in an 11% rise compared to the original material's bandgap (Section S6). Subsequently, the reduction in light absorption by the increased bandgap (Caballero 2003) and the amount of organic material adhered to the particles decreased the efficiency of the phototransesterification process.

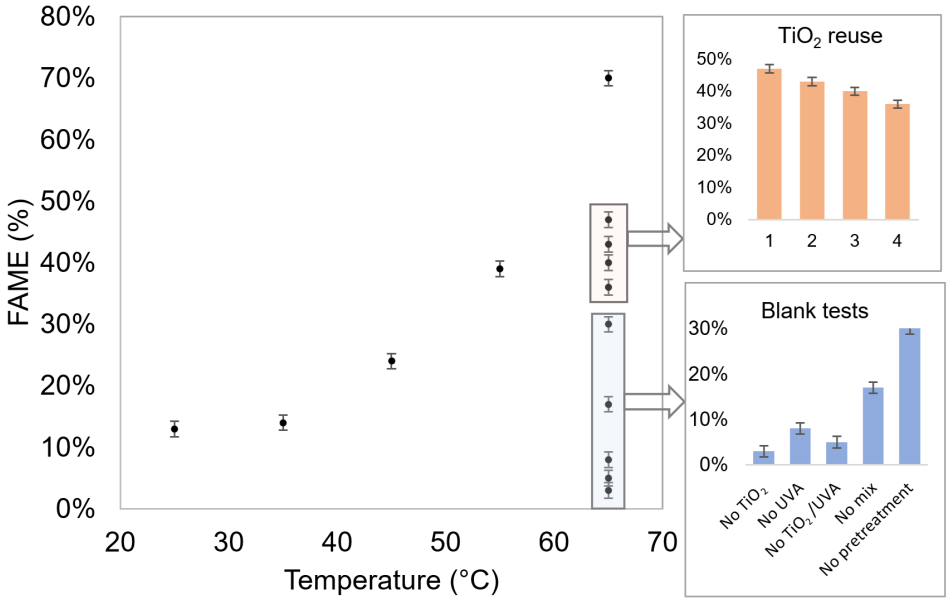


FIGURE 5 | Conversion of canola oil to FAME as a function of reaction temperature (25°C–65°C) under photocatalytic conditions. Error bars represent standard deviation. Insets show (top) catalyst reuse performance over four cycles and (bottom) blank tests conducted at 65°C under different conditions: Absence of TiO_2, absence of UVA irradiation, absence of both catalyst and light, no mixing and no pretreatment. Reaction conditions: Triglyceride (TGL) to methanol molar ratio of 1:55, 20 wt% TiO_2 ($w_{catalyst}/w_{TGL}$), and UVA irradiation.

17571707, 2026, 6, Downloaded from https://onlinelibrary.wiley.com/doi/10.1111/gcbb.70113 by James Cook University, Wiley Online Library on [10/11/2026]. See the Terms and Conditions (https://onlinelibrary.wiley.com/terms-and-conditions) on Wiley Online Library for rules of use; OA articles are governed by the applicable Creative Commons License

4.2 | Canola Oil Transesterification

A series of transesterification reactions of canola oil and methanol using TiO_2 as the photocatalyst was conducted in a batch reactor at temperatures between 25°C and 65°C. Moreover, the influence of light (UVA vs. sunlight), TiO_2 content, and mixing was examined (Figure 5, Section S1). Whilst maintaining the same operational parameters (20% TiO_2 $w_{catalyst}/w_{TGL}$, 30 min of catalyst pretreatment, 4 h of reaction, and UVA irradiation) except for the reaction temperature, it was found that the conversion has a strong dependency on the reaction temperature. As a result, the maximum yield (73% ± 1.41%, Table 4) was achieved at 65°C.

The same operational conditions, but employing ethanol instead of methanol, resulted in a lower conversion of 38%. Despite triglycerides exhibiting greater solubility in ethanol compared to methanol, reactions involving methanol typically yield higher conversion rates compared to alcohols with longer carbon chains (Ayadi et al. 2021). As methanol possesses higher polarity, a lower boiling point and better electron donation ability, it reacts preferentially over ethanol during photocatalysis (Ayadi et al. 2021; Silva et al. 2015).

The biodiesel produced by photocatalysis was compared with that obtained by two conventional thermal processes using acidic and alkaline conditions. Acid catalysis resulted in approximately 100% of FAME and FAEE by simultaneous esterification and transesterification. Esterification was confirmed by a reduction of the FFA content (Table 5). Alkali catalysis furnished 91% of FAME from transesterification, but substantial esterification did not take place significantly, as evidenced by the comparable FFA levels observed before and after the reaction (Table 5). Compared with other studies (Table 3), the results obtained reveal that TiO_2, without further modification

TABLE 4 | Comparison of biodiesel synthesis conditions between the present study and literature data.

	Catalyst	$w_{catalyst}/w_{TGL}$ (%)	Alcohol	Molar ratio	T (°C)	Time (min)	FAAE (%)	References
Synthesis by oxides as catalysts								
Canola oil	TiO_2 + UVA	20	Methanol	55	65	240	73	This study
Canola oil	TiO_2 + sunlight	20	Methanol	55	65	360	19	This study
Canola oil	TiO_2 + UVA	20	Ethanol	55	65	240	38	This study
Canola oil	$HSiW/Al_2O_3$	3	Methanol	27	190	1380	85	Gaurav et al. (2019)
Canola oil	ZnO	12.5	Methanol	27	200	360	35	Pugnet et al. (2010)
Canola oil	$ZnAl/2O_4$	12.5	Methanol	27	200	360	80	Pugnet et al. (2010)
Palm oil	Cu + TiO_2	3	Methanol	20	45	45	91	De and Boxi (2020)
Soybean oil	$SnSO_4$	5	Ethanol	3.5	100	180	70	(Pereira et al. 2014)
Soybean oil	CaO	1.5	Methanol	9	70	180	80	Chen et al. (2020)
Sunflower oil	CaO/ZnO	2	Methanol	10	70	240	95	Lukić et al. (2013)
Sunflower oil	ZrO_2/La_2O_3	15	Methanol	50	200	480	89	Sun et al. (2009)
WCO	CuO/ZnO + UVA	5	Ethanol	9	65	180	93	Guo et al. (2022)
WCO	TiO_2/g-C_3N_4 + sunlight	2	Methanol	9	60	60	84	Khan, Farah, et al. (2021)
WCO	TiO_2 + sunlight	Nanotubes	Methanol	8	60	240	91	Khaligh et al. (2021)
Standard process of biodiesel synthesis								
Canola oil	KOH	—	Methanol	10	90	120	91	This study
Canola oil	H_2SO_4	—	Methanol	10	90	300	99	This study
Canola oil	H_2SO_4	—	Methanol	10	90	60	19	This study

17571707, 2026, 6, Downloaded from https://onlinelibrary.wiley.com/doi/10.1111/gcbb.70113 by James Cook University, Wiley Online Library on [10/11/2026]. See the Terms and Conditions (https://onlinelibrary.wiley.com/terms-and-conditions) on Wiley Online Library for rules of use; OA articles are governed by the applicable Creative Commons License

TABLE 5 | Characterisation of canola oil and FAME obtained by acid, alkali and photocatalysis.

			FAME (catalyst)		
		Canola oil	**Acid**	**Alkali**	**Photo**
FAME	mol%	—	99	91	73 (±1.41)
FFA	%	1.2 (±0.2)	0.1 (±0.1)	0.9 (±0.2)	0.4 (±0.2)
Boiling point 1[a,c]	°C	—	254	251	246
	Mass loss (%)	—	99	95	75
Boiling point 2[b,c]	°C	421	—	400	400
	Mass loss (%)	99	—	3	23
Flash point[d]	°C	283	161	160	160
Ignition temperature (T_I)[c]	°C	383	217	215	216
Burnout temperature (T_B)[c]	°C	454	258	263	257
Maximum combustion rate (C_{max})[c]	$(dM/dT)_{max}$	1.81	2.24	1.90	1.49
E_a°	kJ/mol	30.33	30.17	32.89	30.33
A	—	0.13	0.25	0.21	0.15
R^2 of E_{aTGA} linear model	—	0.981	0.982	0.966	0.981

[a]In accordance with ASTM D6751-15 (ASTM International 2015): minimum of 130°C.
[b]In accordance with ASTM D7398 (ASTM International 2016): 100°C–615°C.
[c]Error: ±0.69.
[d]In accordance with ASTM D98 (ASTM International 2017a): minimum of 120°C.

but with an adequate pretreatment and proper operational conditions, can effectively catalyse phototransesterification and photoesterification.

When the light source was changed to sunlight with otherwise identical operating conditions, the process demonstrated a reduced efficacy (19%) compared to that with UVA light (73%). A lower conversion was expected as TiO_2 activation requires UVA light with a wavelength between 388 nm (anatase) and 410 nm (rutile) (Pawar et al. 2018), which represents only a small percentage of the sun's radiation (Kanakaraju et al. 2016). In addition, the solar irradiation profile measured during the experiments (Figure S1) indicates that the effective UVA flux was both lower and more variable than the controlled emission of the Rayonet reactor, further contributing to the reduced reaction rate. This behaviour is consistent with the measured bandgap of the catalyst, which confirms that the material is primarily active in the UVA region. To improve solar application, catalyst modification strategies could be considered, such as non-metal doping strategies (e.g., N or C) to reduce the bandgap (Ansari et al. 2016; Asahi et al. 2001), coupling with visible-light sensitizers (Pelaez et al. 2012), and the development of heterojunction systems to enhance charge separation and extend absorption into the visible region (Li et al. 2021).

The blank tests confirm that favourable operating conditions are necessary to achieve high yields. The test with TiO_2 without pre-treatment resulted in a moderate conversion (30%) compared with the other operating parameters evaluated. In the absence of stirring, a poor conversion of just 17% was likewise observed. In both cases, the drops in efficiency were caused by ineffective mass transfer. Moreover, light activation was crucial as the conversion rate dropped to less than 10% in the dark.

Even when employing optimal operational conditions, the reuse of recovered TiO_2 caused a steady drop in its photocatalytic performance. Nevertheless, a conversion of 36% was still maintained after a total of 5 cycles. It is well-established that residual organic materials create a passivating film on the catalyst surface, thereby blocking its pores and diminishing light penetration (Welter, Santana, et al. 2022). In fact, reductions in catalytic effectiveness are commonly observed during reusage studies, as shown in Table 4 and further discussed in Section 4.2 and confirmed by Gardy et al. (2017).

After the first cycle, the global mass balance was calculated considering the organic material (reactants and products) present in the reactional medium and trapped within the pores. Carboxylic species are known to bind strongly to TiO_2 surfaces, which justifies the alcohol pretreatment step employed to pre-fill the pores and reduce initial adsorption of reactants. Based on that, an overall conversion of 69% was found. However, as discussed further in Section 4.2, a large amount of organic material comprising 89% of canola oil (33% of the total mass, Table 5) was retained inside the catalyst. This finding suggests that the pores were probably obstructed at the onset of the reaction. Thus, it was therefore assumed that only the free organic material participated in the reaction. Following this assumption, a nominal conversion of 73% (±1.41) was achieved.

4.3 | FAME Characterisation

Various analytical methods (Table 5) were employed to characterise the feedstock (canola oil) and reaction products (FAME). The composition of the photocatalysis-derived product was

17571707, 2026, 6, Downloaded from https://onlinelibrary.wiley.com/doi/10.1111/gcbb.70113 by James Cook University, Wiley Online Library on [10/11/2026]. See the Terms and Conditions (https://onlinelibrary.wiley.com/terms-and-conditions) on Wiley Online Library for rules of use; OA articles are governed by the applicable Creative Commons License

also compared with that obtained through conventional thermal techniques (acid and alkali catalyses). The conversion of TGL to FAME was assessed using ^{1}H-NMR spectroscopic analysis (Figure S.5) and monitored via FTIR-ATR spectroscopy (Figure S.16). The ATR-FTIR spectra of canola oil and the various FAME products exhibited notable similarities in their infrared regions, particularly in the ester carbonyl stretching band v(C═O) at ~1740 cm^{-1}, the C—O—C stretching vibrations at ~1160–1190 cm^{-1}, the aliphatic C—H stretching bands at ~2850–2920 cm^{-1}, and the v(C═C) band near ~3006 cm^{-1} (details are given in Table S.8). Titration was used to determine the FFA content, which was found to be 1.2% for canola oil. The corresponding values for the various FAMEs were 0.2% for acid catalysis, 0.9% for alkali catalysis, and 0.6% for photocatalysis. These results indicate that acid catalysis likely involves partial esterification of FFA, leading to a reduction in %FFA and an increase in FAME conversion. In contrast, alkali catalysis appears to primarily involve transesterification, as evidenced by the minimal change in FFA content. During TiO_2-photocatalysis, both photoesterification and phototransesterification processes occur, a finding consistent with those reported by other authors (De and Boxi 2020; Gardy et al. 2017; Khaligh et al. 2021; Mihankhah et al. 2018; Welter et al. 2026; Welter, Santana, et al. 2022; Wen et al. 2009). The %FFA values obtained through titration are consistent with those reported in the literature (Caballero 2003; Shahidi 2005).

The thermogravimetric analysis (TGA, more details in Section S4) showed that canola oil has a degradation peak at 421°C (Figure S.6), while FAME exhibits a peak between 240°C and 250°C. The product resulting from photocatalysis displayed two distinct peaks, one corresponding to FAME and another to unreacted oil, indicating incomplete conversion. The degradation curves of FAME suggest that the products possess high thermal stability. Products characterised by low thermal stability typically exhibit an initial peak in the range of 100°C–150°C, which is associated with volatile compounds (Mostafa and El-Gendy 2017; Wnorowska et al. 2021). Comparable findings were reported by various researchers for FAME derived from soybean oil and babassu (Nicolau et al. 2018), and Croton *melagocarpus* oil (Kivevele et al. 2011).

Thermal parameters such as flash point, T_I, T_B, C_{max} and $E_a°$ were also determined. The flash point denotes the minimum temperature at which vapour can ignite, and flames can spread across the remaining liquid (Abdelkhalik et al. 2018). This point is equivalent to the temperature where 17.5% of the weight is lost (Abdelkhalik et al. 2018) or where 74% of the boiling point temperature is reached (Mofijur et al. 2017). The ASTM D93 (ASTM International 2018) procedure states that the minimum value should be 120°C (Mofijur et al. 2017). A value of 160°C was obtained, which is similar to those found in the literature (Encinar et al. 2018). The ignition temperature (T_i) represents fuel stability during storage (Khan, Park, et al. 2021; Sharma and Singh 2009) and the capacity of vapours to autocombust. The ignition temperature and burnout temperature (T_B, 95% of complete combustion) were similar for FAME products obtained by photocatalysis and traditional catalysis. The maximum combustion rate (C_{max}) revealed that the product from acid catalysis has the highest value with 2.24°C/min. In contrast, the product from photocatalysis showed the lowest value (1.49°C/min), suggesting that the presence of residual TGL may interfere with the thermoanalysis results. The activation energy ($E_a°$) for canola oil and FAME was found to be similar, at 30.33 and 32.89 kJ/mol. This similarity indicates that additional energy is not required to further progress of the reaction. System heat is essential mainly to increase mass transfer between the reactants, which is supported by the thermodynamic parameters discussed later and the literature (Silva et al. 2015; Welter et al. 2026; Welter, Santana, et al. 2022).

The composition of the different transesterification products was furthermore determined by gas chromatography (Table 6). In comparison with traditional methods (acid and alkali catalysts), transesterification by photocatalysis converts the C18:1-carbon chain (oleic acid) more readily than the C18:2 ones (linoleic and linolenic acids). This difference has been attributed to the larger number of double bonds in linoleic and linolenic acids, which increases the energy required for the reaction to occur. This becomes noticeable when comparing the enthalpy of the two most common methyl esters, methyl oleate ($\Delta H°_{r,298K} = 122$ kJ/mol) and methyl linoleate ($\Delta H°_{r,298K} = 245$ kJ/mol), respectively (Smith and Martell 2004).

TABLE 6 | FAME composition[a] obtained from canola oil-methanol transesterification using different catalysts.

			FAME (catalyst)		
		Canola oil	Acid	Alkali	Photo
Unreacted canola oil		**Raw material**	**1%**	**9%**	**27%**
Methyl palmitate	C16:0	4%	4%	5%	4%
Methyl stearate	C18:0	3%	2%	2%	2%
Methyl oleate (9)	C18:1	59%	60%	59%	70%
Methyl oleate (11)	C18:1	2%	3%	3%	3%
Methyl linoleate	C18:2	21%	20%	20%	14%
Methyl linolenate	C18:2	9%	9%	9%	5%
Methyl eicosonate	C20:1	2%	1%	0%	0%
Methyl eicosadienoate	C20:2	2%	1%	1%	1%

[a]Obtained by G.C. (Section S5).

17571707, 2026, 6, Downloaded from https://onlinelibrary.wiley.com/doi/10.1111/gcbb.70113 by James Cook University, Wiley Online Library on [10/11/2026]. See the Terms and Conditions (https://onlinelibrary.wiley.com/terms-and-conditions) on Wiley Online Library for rules of use; OA articles are governed by the applicable Creative Commons License

TABLE 7 | Composition of intermediate products obtained during canola oil–methanol transesterification using different catalysts.

			FAME (catalyst)				
			Acid		Alkali	Photo	
		Canola oil	1 h	5 h	2 h	1 h	5 h
#	Unreacted canola oil	100%	85%	1%	9%	85%	27%
1	Glycerol	0%	0%	0%	0%	0%	0%
2	Other esters	0%	3%	24%	21%	2%	27%
3	Methyl oleate	0%	10%	65%	63%	11%	41%
4	Methyl linoleate	0%	4%	6%	5%	2%	3%
6	Monoolein	0%	0%	0%	0%	0%	0%
7	1-Oleoyl glycerol	0%	1%	1%	0%	0%	1%
9	1,2-Dioleoyl glycerol	1%	3%	1%	1%	0%	2%
10	1,3-Diolein	3%	6%	1%	8%	0%	3%
11	Glyceryl trioleate	43%	32%	1%	9%	31%	3%
12	Other triglycerides	52%	42%	1%	0%	47%	13%

4.4 | Identification of MG and DG Intermediates

The possible presence of reaction intermediates, that is monoacylglycerol (MG) and diacylglycerol (DG), was investigated experimentally (NMR and GC) in comparison with literature data (Galvan et al. 2020; Nieva-Echevarría et al. 2015). Analyses were conducted using the products obtained from acid catalysis and photocatalysis, focusing on those with the highest conversion rates as well as those from shorter reaction periods, which yielded lower conversions and incomplete reactions. Lower FAME conversions (~15%) were observed for both methods, which supports the possible presence of MG and DG. As expected, other studies have reported higher amounts of MG and DG at the beginning of the reaction, with correspondingly lower concentrations of FAME (Ferrão-Gonzales et al. 2011; Noureddini and Zhu 1997). For example, Pugnet and co-workers monitored the transesterification of rapeseed oil with methanol over 6 h but could detect small concentrations of MG and DG only within the first 2 h of the reaction (Pugnet et al. 2010).

GC (Table 7) analyses indicated the presence of MG at a maximum concentration of 1% in all samples. The concentration of DG varied depending on the process employed. For the incomplete acid-catalysed reaction, a total of 9% of DG was found, whereas photoesterification yielded approximately 5%. Reactions utilising acid and alkali catalysts produced final products containing primarily fatty acid methyl esters (FAME), MG, DG and triglycerides (TGL). In contrast, photocatalysis resulted in small quantities of various unidentified compounds, collectively accounting for 9% of the product. However, each of these unknown compounds individually constitutes less than 1% of the total composition. This suggests that although secondary reactions occur in the background, they do not significantly impact the production of esters.

Analysis using ^{1}H-NMR (Figure 6) revealed that the crude products obtained from acid catalysis contained traces of MG and DG, despite the low 15% conversion rate. The analysis focused on the glyceridic region (δ 3.5–5.5 ppm), where characteristic resonances of mono- and diglycerides are observed. Signals attributed to MG and DG (typically appearing at δ ~3.65–3.75 ppm and 4.05–4.30 ppm) were detected in low-conversion samples. After prolonged reaction times and consequently higher conversions, TGL was fully converted into FAME in the acid-catalysed system, with no detectable intermediates (99% of FAME, Figures 7 and 8). At this stage, the glyceridic signals disappeared, while the methoxy signal of FAME at δ ~3.63 ppm became dominant, indicating complete conversion within the detection limit of the technique. In comparison, trace amounts of intermediates (MG and DG) were detected in the photocatalysis product (Figures 7 and 8) for higher conversion (73%) but not at lower conversion (15%, Figure 6).

Noureddini and Zhu (1997) investigated the transesterification of soybean oil with methanol using KOH as the catalyst (Noureddini and Zhu 1997). The amounts of MG and DG detected were negligible compared with FAME. Likewise, Albuquerque Andrade et al. (2011) evaluated the transesterification of buriti oil, and the isolated product consisted of 94% of FAME, 3.27% of MG, and 0.98% of DG, respectively (Andrade et al. 2011). Ferrão-Gonzales et al. (2011) assessed the presence of intermediates for the transesterification of rapeseed oil by *Candida antarctica* B lipase (Ferrão-Gonzales et al. 2011). Although the reaction was slow (10–24 h), only trace concentrations of MG and DG were found. Hence, MG and DG may not represent significant components of the crude product, but their presence in trace amounts may still interfere with the reactants' miscibility (Chen et al. 2020). Triglycerides are poorly miscible to practically insoluble in methanol phases. DG and MG may thus act as surfactants, improving mixing between the oil and methanol. Chen et al. (2020) performed the transesterification of soybean oil with methanol using CaO as a catalyst. The authors reported that oil and methanol initially separated into two phases, but the separation rate decreased drastically after the addition of MG and DG. This behaviour can be attributed to the

17571707, 2026, 6, Downloaded from https://onlinelibrary.wiley.com/doi/10.1111/gcbb.70113 by James Cook University, Wiley Online Library on [10/11/2026]. See the Terms and Conditions (https://onlinelibrary.wiley.com/terms-and-conditions) on Wiley Online Library for rules of use; OA articles are governed by the applicable Creative Commons License

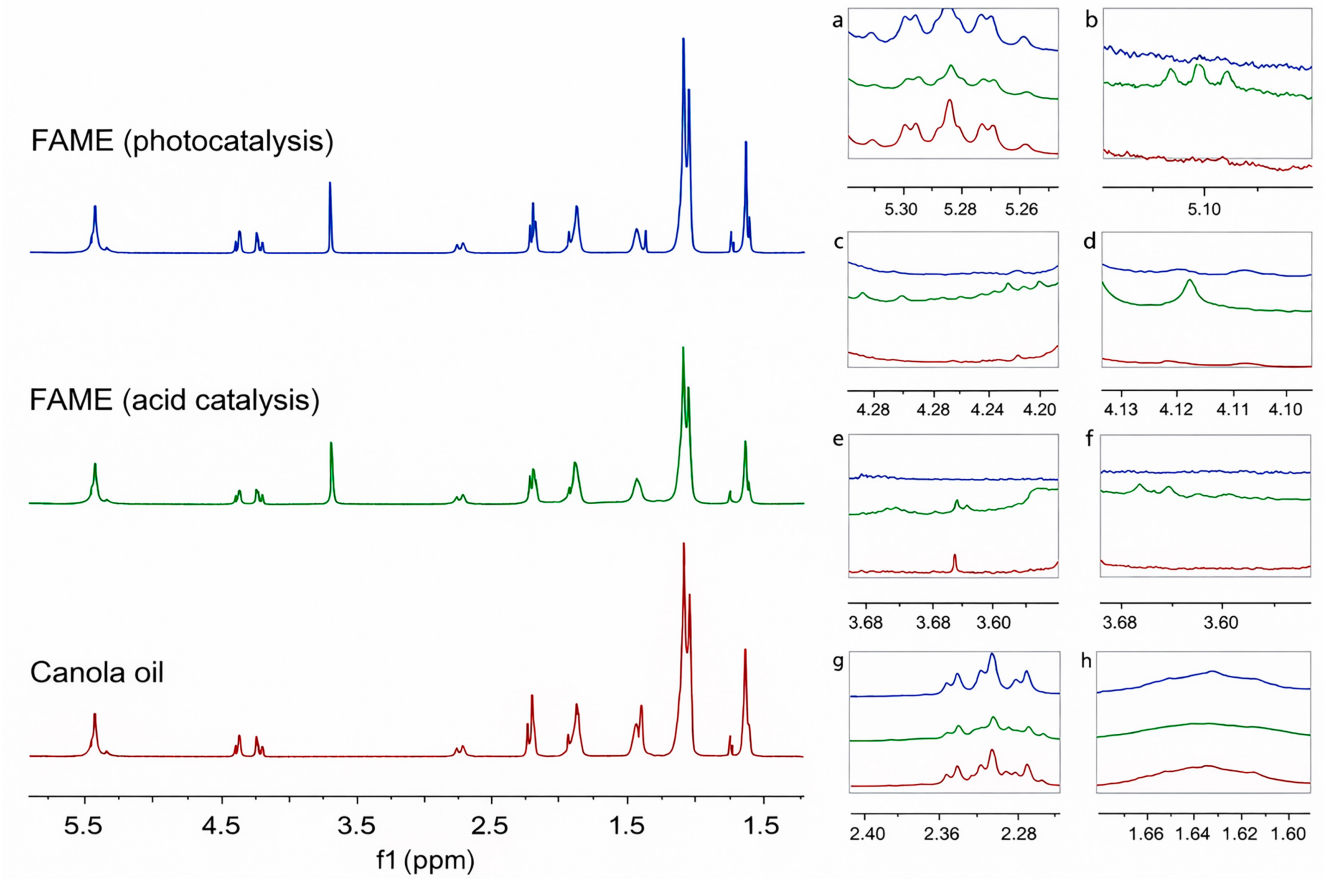


FIGURE 6 | ^{1}H NMR spectra (400 MHz, $CDCl_3$) of canola oil and FAME obtained via photocatalysis and acid-catalysed transesterification (15% conversion). The spectra compare the chemical profiles of the initial oil and partially converted products. Insets (a–h) highlight expanded spectral regions corresponding to signals associated with mono- and diglycerides.

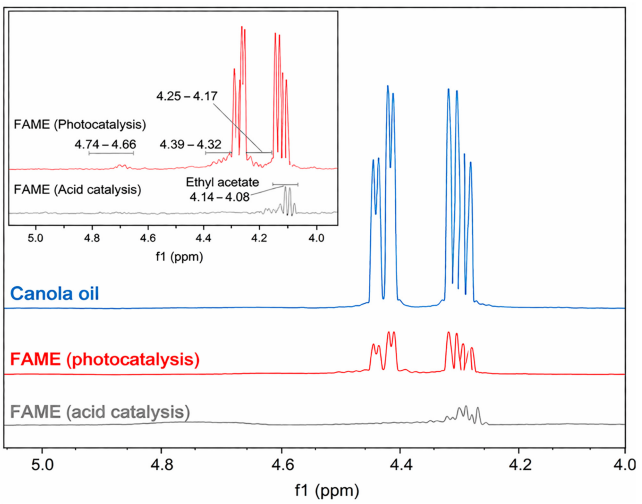


FIGURE 7 | ^{1}H NMR spectra (400 MHz, $CDCl_3$) in the region $\delta = 4.40–4.00$ ppm of canola oil and FAME obtained via photocatalysis and acid-catalysed transesterification (73% conversion). This region highlights signals associated with ester functionalities and intermediates. Residual ethyl acetate is observed in the product obtained by acid catalysis, indicating differences in reaction pathways or purification efficiency.

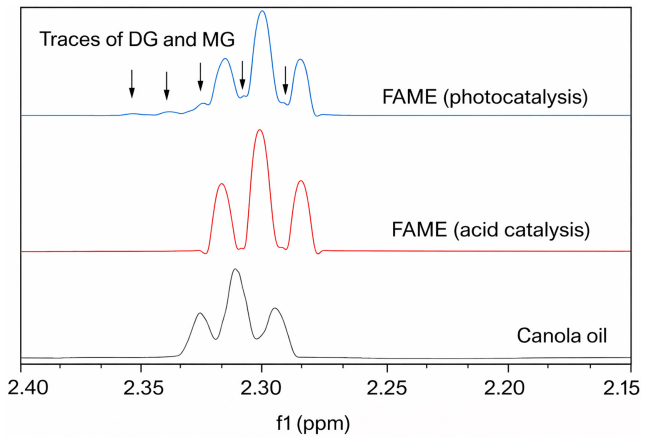
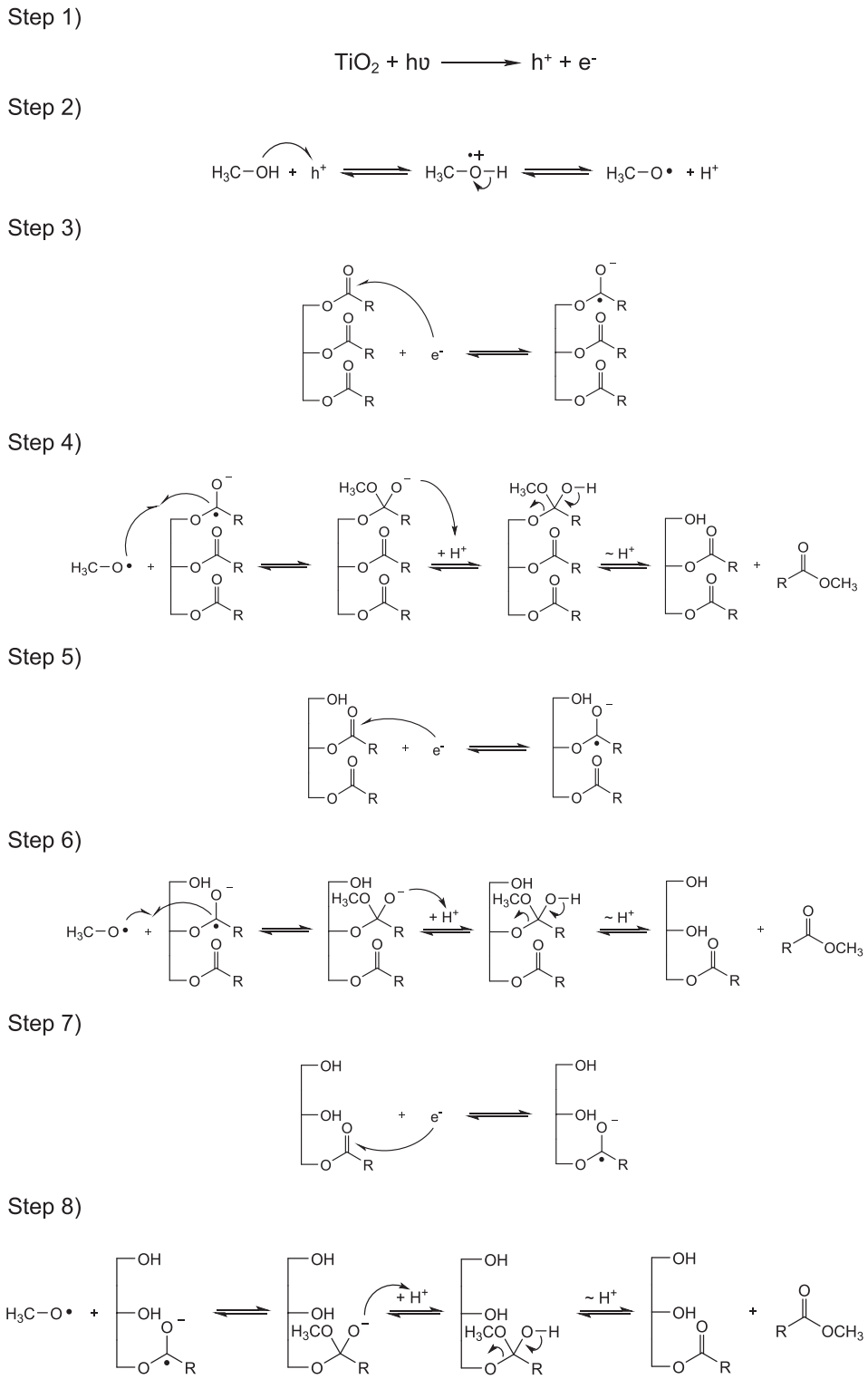


FIGURE 8 | ^{1}H NMR spectra (400 MHz, $CDCl_3$) in the region $\delta = 2.40–2.25$ ppm of canola oil and FAME obtained via photocatalysis and acid-catalysed transesterification (73% conversion). This region highlights signals associated with glyceride moieties. Traces of mono- and diglycerides (MG and DG) are observed in the photocatalytic product, suggesting incomplete conversion and the presence of reaction intermediates during transesterification.

amphiphilic structure of these intermediates, which contain polar hydroxyl groups and non-polar hydrocarbon chains. Such a molecular configuration enables them to act at the oil–alcohol interface, effectively bridging the polar methanol phase and the non-polar triglyceride phase. As a result, interfacial tension is reduced and phase contact is improved, facilitating mass

17571707, 2026, 6, Downloaded from https://onlinelibrary.wiley.com/doi/10.1111/gcbb.70113 by James Cook University, Wiley Online Library on [10/11/2026]. See the Terms and Conditions (https://onlinelibrary.wiley.com/terms-and-conditions) on Wiley Online Library for rules of use; OA articles are governed by the applicable Creative Commons License



SCHEME 1 | Proposed phototransesterification mechanism for canola oil (TGL) and methanol photocatalysed by TiO_2 (*R*=cis-$CH_3(CH_2)_7CH{=}CH(CH_2)_7$). Order of each transesterification step may vary.

transfer. Under the experimental conditions employed in this work, this interfacial effect, combined with strong agitation, is consistent with the pseudo-homogeneous kinetic behaviour observed, thereby supporting the use of a homogeneous kinetic model despite the heterogeneous catalytic system.

4.5 | Proposed Photoreaction Mechanism

Photocatalysis proceeds via transesterification of TGL and, to a lesser extent, esterification of residual FFA. However, esterification is not further discussed because of the small amounts of

17571707, 2026, 6, Downloaded from https://onlinelibrary.wiley.com/doi/10.1111/gcbb.70113 by James Cook University, Wiley Online Library on [10/11/2026]. See the Terms and Conditions (https://onlinelibrary.wiley.com/terms-and-conditions) on Wiley Online Library for rules of use; OA articles are governed by the applicable Creative Commons License

FFA in the feedstock (1.2% ± 0.2). Scheme 1 shows the proposed mechanism for TGL (triolein) phototransesterification with methanol. TiO_2 excitation by photons ($h\nu$) with enough energy to overcome the bandgap causes charge separation (Step 1) (Manique et al. 2016; Micic et al. 1993). Electrons (e^-) are promoted to the conduction band (CB), generating positive holes (h^+) in the valence band (VB) (Ohtani 2011). Both charge carriers (h^+ and e^-) react with methanol (Step 2) or with adsorbed TGL (Step 3) on the catalyst surface, generating a methoxy radical ($^{\cdot}OCH_3$) and an acyl radical species ($RCO_2R'^-$). Subsequent radical combination and elimination yields the first intermediate, diacylglycerol (DG, diolein), and one molecule of methyl oleate, RCO_2CH_3, (Step 4). Successive transesterification of diacylglycerol results in monoacylglycerol (MG, monoolein) and a second molecule of methyl oleate (Steps 5 and 6). The monoacylglycerol is further converted by the same mechanism to the third methyl oleate molecule and glycerol (Step 7). Similar mechanistic pathways have been proposed for the TGL phototransesterification catalysed by TiO_2 supported on graphene (Borah et al. 2018), and by TiO_2 (Welter, Santana, et al. 2026); and for FFA photoesterification and TGL phototransesterification (Ghani et al. 2020; Guo et al. 2021; Welter et al. 2026; Welter, Santana, et al. 2022). However, alternative phototransesterification mechanisms have likewise been proposed (Alsharifi et al. 2017; Yan et al. 2009).

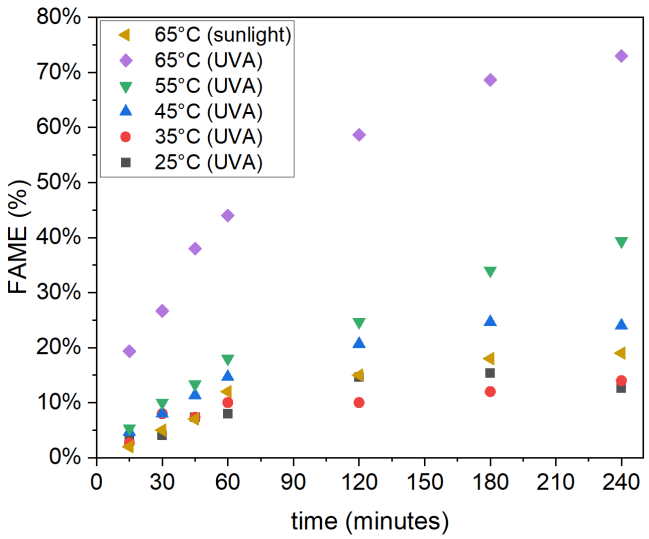


FIGURE 9 | Conversion of canola oil to FAME as a function of reaction time under photocatalytic conditions using TiO_2. Experiments were conducted at temperatures ranging from 25°C to 65°C under UVA irradiation, with additional tests at 65°C under sunlight. The results highlight the influence of temperature and irradiation source on reaction kinetics. Reaction conditions: Triglyceride (TGL) to methanol molar ratio of 1:55 and 20 wt% TiO_2 ($w_{catalyst}/w_{TGL}$).

The proposed mechanism is in agreement with the experimental results achieved in this work, such as the strict dependence on both light and catalyst (blank tests, details are found in Section 4.2), exclusive FAME formation under irradiation conditions (details are found in Section 4.3), and pseudo-homogeneous kinetic behaviour identified by the best-fitting model (details are found in Section 4.6).

4.6 | Kinetics and Thermodynamics Properties

Kinetic curves were subsequently obtained for the phototransesterification of canola oil with methanol under UVA irradiation (Figure 9, 1 mol TGL:55 mol MeOH, 20% TiO_2 $w_{catalyst}/w_{TGL}$ temperature range: 25°C–65°C, 4 h). High temperatures were found desirable for achieving a high transesterification efficiency. The highest conversion of 73% (±1.41) was achieved at 65°C. The gap between conversions achieved at 55°C and 65°C was approximately 33%. This significant difference can be attributed to the increased miscibility of the reagents and hence mass transfer at elevated temperatures. Six kinetic models were evaluated (Equations 15–20, Section 3), and their statistical analyses are listed in Table 8. The F2B4 model, which considers the forward reaction as second-order and the backward reaction as fourth-order, provided the best fit with the experimental data (Figure 10). Both reaction constants (k_1 and k_{-1}) were consequently obtained using this model (Figure 10). The intermediates (MG and DG) were disregarded due to their neglectable concentrations, as discussed in Section 4.4. The solar phototransesterification conducted at 65°C showed a significantly lower conversion over time, most likely due to the limited UV fraction within the solar spectrum and the intrinsic bandgap limitation of TiO_2 (Khezrianjoo and Revanasiddappa 2012; Rajeshwar et al. 2008).

The thermodynamic properties of the phototransesterification reaction were furthermore determined (Table 9). Although all the models showed convergence values higher than 0.95, only F2B4 (with the best accuracy) resulted in consistent data, as shown in Table 9. Models that considered lower orders (first and second) resulted in negative values of E_a for the backward reaction. The F1B3 model gave a low convergence for enthalpy and

TABLE 8 | Kinetic model statistical analysis applied to the experimental kinetic data obtained for the phototransesterification of canola oil and considering FAME and feedstock kinetic curves.

Model	R^2	$F(1,38)$	SD	B	$t(38)$	p
F1B1	0.971	5297	0.015	0.971	59.354	< 0.001
F1B2	0.995	7557	0.013	0.997	86.830	< 0.001
F2B2	0.972	5413	0.020	0.973	59.930	< 0.001
F1B3	0.972	5114	0.021	0.973	66.268	< 0.001
F2B4	0.996	8969	0.012	0.998	97.700	< 0.001
L–H	0.971	5778	0.021	0.970	60.029	< 0.001

17571707, 2026, 6, Downloaded from https://onlinelibrary.wiley.com/doi/10.1111/gcbb.70113 by James Cook University, Wiley Online Library on [10/11/2026]. See the Terms and Conditions (https://onlinelibrary.wiley.com/terms-and-conditions) on Wiley Online Library for rules of use; OA articles are governed by the applicable Creative Commons License

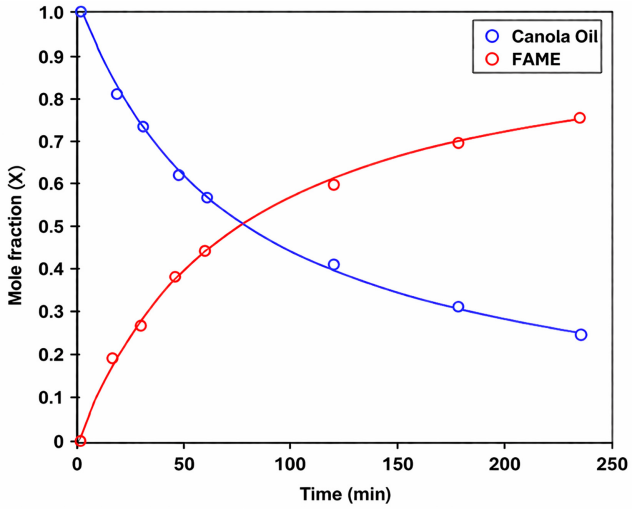


FIGURE 10 | Kinetic modelling of canola oil phototransesterification using the F2B4 model. Experimental data (symbols) and corresponding model fits (lines) describe the decrease in canola oil fraction and the formation of FAME over time. Reaction conditions: Triglyceride (TGL) to methanol molar ratio of 1:55, 20 wt% TiO_2 ($w_{catalyst}/w_{TGL}$), 65°C, under UVA irradiation.

entropy. Nevertheless, the F2B4 model produced higher convergence for all parameters, and was thus considered the most satisfactory and was used for further discussion. The E_a value for the forward reaction (60.27 kJ/mol) can be considered small compared to that of the backward reaction (233.71 kJ/mol) and indicates the high efficiency of the catalyst (Encinar et al. 2018). The Van't Hoff model (Equation 12) was used to obtain ΔS and ΔH. The value of ΔH of 83.50 kJ/mol indicates the endothermic nature of the reaction, as observed by other authors (Zanjani et al. 2020). The increased conversion with increasing temperature also suggests an endothermic reaction. Moreover, increasing temperature improves the reagents' miscibility, resulting in higher conversion. For the oleic acid-methanol esterification, increasing temperature is more relevant for miscibility than for the reaction energy supply requirement (Silva et al. 2015; Welter, Santana, et al. 2022). The ΔS of 0.27 kJ/mol K ($\Delta S > 0$) indicates that the system's entropy is increasing, and the reaction tends to become irreversible (Zanjani et al. 2020). ΔG (Figure 11) suggests that the reaction is favoured at higher temperatures, which is confirmed by the decrease in Gibbs free energy with increasing temperature.

5 | Outlook and Scale-Up Considerations

To amplify the developed photocatalytic transesterification process from laboratory to industrial scale, a process-level assessment must be considered beyond the conversion itself. Through process optimisation it was possible to reach up to 73% of conversion, reuse the catalyst, and reduce waste to almost zero. However, scale-up should focus on key parameters such as light penetration, catalyst activity, multiphase mass transfer, environmental impact, and costs.

The scale-up of photocatalytic systems is fundamentally constrained by photon transport, as light absorption and scattering lead to exponential attenuation of photon flux, according to the Beer–Lambert law, resulting in a considerable decay of photons across the path length, poorly illuminated regions, termed 'dark zones', and, as a consequence, reduced volumetric productivity in larger reactors (Braham and Harris 2009; Chandhinipriya and Ranjitha 2025). To maintain high photon flux and minimise optical attenuation, thin-film configurations, such as microreactors, have been proposed for photocatalytic scale-up (Cassano and Alfano 2000; Oelgemöller 2012; Van Gerven et al. 2007; Welter Jr., de Souza, et al. 2022). Solar microreactor systems (3 wt% catalyst, oil-to-methanol ratio 1:2, solar irradiation, glass microreactors) produced more than 90% biodiesel from waste cooking oil and reduced energy consumption by up to 94% compared to the conventional thermal processes (Aghel and Biabani 2024). Other strategies focus on spectral and optical management. One option is the use of luminescent solar concentrators, which redistribute incident radiation and increase effective photon flux (Cambié et al. 2017; Malato et al. 2002; Van Gerven et al. 2007; Zhao et al. 2017). Another option is catalyst immobilisation, which minimises light scattering by suspended particles and maintains the flux uniform across the active surface (Byrne et al. 1998; He et al. 2025; Pozzo et al. 1997).

The heterogeneous nature of the oil–alcohol–catalyst system introduces multiphase mass transfer resistances. Although at laboratory scale, under vigorous mix, the system was considered pseudo-homogeneous, at large scale the internal and external mass diffusion resistances are more significant and might drive the system kinetics (Atadashi et al. 2013; Demirbas 2009; Leung et al. 2010). This behaviour is observed in laminar liquid-phase photoreactors operated under high light intensity (Salvadó-Estivill et al. 2007). One strategy to overcome miscibility limitations is the use of co-solvent, such as ethanol in the system oil-methanol-catalyst (Encinar et al. 2007; Zhou et al. 2006). Boocock et al. (1996) evaluate the synthesis of biodiesel using soybean oil and methanol (1:6 M ratio) at 40°C. The biphasic system required about 1 h to reach 95 of conversion. However, by adding an organic co-solvent (tetrahydrofuran—THF), the system resulted in a single-phase and the same efficiency was reached after only 10 min. Thanh et al. (2013) produced biodiesel from WCO (1 wt% NaOH, methanol-to-oil molar ratio 4.5:1, 25°C, 30 min) using acetone as co-solvent (25 wt% acetone to oil) and achieved 98 of conversion, while the absence of co-solvent resulted in only 55 of conversion after 60 min. Another strategy is high-shear mixing or ultrasonic irradiation to reduce interfacial mass transfer resistance and increase catalyst-reactant contact (Colucci et al. 2005; Thanh et al. 2012). Reactor designs need to address both external mass transfer (liquid film to the catalyst) and internal diffusion when immobilised supports or porous catalysts are used (Kouzu and Hidaka 2012; Oyekunle et al. 2023). Other strategies to improve mass transfer include reactor geometry optimisation to reduce dead zones (Mueses et al. 2013; Pérez et al. 2006), and maintaining a temperature of about 65°C uniformly throughout larger volumes while accounting for heat generation from exothermic transesterification and photon absorption (Freedman et al. 1984; Noureddini and Zhu 1997).

Under natural sunlight, conversion decreases substantially due to spectral mismatch, since only approximately 4%–5%

17571707, 2026, 6, Downloaded from https://onlinelibrary.wiley.com/doi/10.1111/gcbb.70113 by James Cook University, Wiley Online Library on [10/11/2026]. See the Terms and Conditions (https://onlinelibrary.wiley.com/terms-and-conditions) on Wiley Online Library for rules of use; OA articles are governed by the applicable Creative Commons License

TABLE 9 | Kinetic and thermodynamic parameters obtained by different mathematical models.

Model	k_{-1}[a]	k_1[a]	K^a_{eq}	E_a[b] (kJ/mol)	A[c]	E_a[d] (kJ/mol)	A[e]	$\Delta G^{a,d}$ (kJ/mol)	$\Delta G^{a,e}$ (kJ/mol)	ΔH (kJ/mol.K)	ΔS (kJ/mol)
F1B1	3.4E-03	1.1E-02	3.2E-01	26.88 (R^2: 0.709)	100.73 (R^2: 0.709)	−35.81 (R^2: 0.740)	1.02E-8 (R^2: 0.740)	−3.24 (p_v: 0.110)[f] (t_v: 1.795)	2.01 (p_v: 0.110) (t_v: 1.795)	−62.68 (R^2: 0.863)	−0.19 (R^2: 0.863)
F1B2	9.7E-03	1.1E-02	8.8E-01	28.91 (R^2: 0.911)	1.8E+02 (R^2: 0.911)	−64.19 (R^2: 0.715)	1.54E-12 (R^2: 0.715)	−5.67 (p_v: 0.086) (t_v: 1.960)	−8.29 (p_v: 0.086) (t_v: 1.960)	117.14 (R^2: 0.915)	0.37 (R^2: 0.915)
F2B2	3.1E-04	3.4E-02	9.0E-03	30.28 (R^2: 0.706)	1.00E+3 (R^2: 0.706)	−82.22 (R^2: 0.764)	1.50E-16 (R^2: 0.764)	−13.23 (p_v: 0.302) (t_v: 1.204)	9.37 (p_v: 0.302) (t_v: 1.204)	−112.49 (R^2: 0.775)	−0.36 (R^2: 0.775)
F1B3	3.2E-02	3.3E-02	1.0E+00	60.29 (R^2: 0.840)	3.96E+7 (R^2: 0.840)	241.28 (R^2: 0.321)	1.52E+12 (R^2: 0.321)	−0.08 (p_v: 0.081) (t_v: 1.9987)	−14.97 (p_v: 0.081) (t_v: 1.9987)	123.65 (R^2: 0.447)	0.41 (R^2: 0.447)
F2B4	3.1E-03	3.3E-02	9.3E-02	60.27 (R^2: 0.839)	3.92E+07 (R^2: 0.839)	233.71 (R^2: 0.791)	1.44E+18 (R^2: 0.791)	−6.88 (p_v: 0.002) (t_v: 4.257)	−4.72 (p_v: 0.002) (t_v: 4.257)	83.50 (R^2: 0.870)	0.27 (R^2: 0.870)
L–H	6.0E-01	1.9E-02	2.7E+02	89.92 (R^2: 0.902)	3.50E-16 (R^2: 0.902)	−80.38 (R^2: 0.839)	2.55E+13 (R^2: 0.839)	15.69 (p_v: 0.947) (t_v: 0.069)	−11.25 (p_v: 0.947) (t_v: 0.069)	175.58 (R^2 = 0.902)	0.55 (R^2 = 0.840)

[a]Temperature: 338.15 K.
[b]Forward.
[c]Van't Hoff model.
[d]Backward.
[e]$\Delta G = f(\Delta H, T, \Delta S)$.
[f]p_v: p-value and t_v: t-value.

17571707, 2026, 6, Downloaded from https://onlinelibrary.wiley.com/doi/10.1111/gcbb.70113 by James Cook University, Wiley Online Library on [10/11/2026]. See the Terms and Conditions (https://onlinelibrary.wiley.com/terms-and-conditions) on Wiley Online Library for rules of use; OA articles are governed by the applicable Creative Commons License

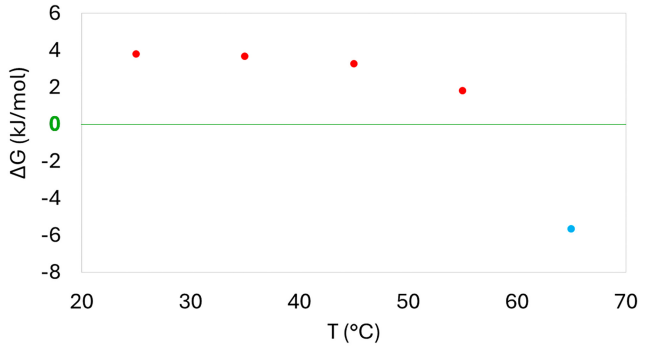


FIGURE 11 | Gibbs free energy (ΔG) as a function of temperature for the phototransesterification of canola oil with methanol, estimated using the F2B4 kinetic model. The results indicate the thermodynamic favourability of the reaction at different temperatures. Reaction conditions: Triglyceride (TGL) to methanol molar ratio of 1:55 and 20 wt% TiO_2 ($w_{catalyst}/w_{TGL}$).

of solar radiation lies in the UVA region required for TiO_2 activation (Fujishima et al. 2008; Herrmann 2010; Mueses et al. 2013; Pérez et al. 2006; Yurdakal et al. 2008). This motivates the development of visible-light-active photocatalysts and spectral-conversion systems. Heterojunction materials have already demonstrated improved solar performance: TiO_2/20% g-C_3N_4 achieved 89.5% yield at 60°C (1:9 oil: methanol molar ratio, 1 h) (Khan, Farah, et al. 2021), a g-C_3N_4–TiO_2@montmorillonite S-scheme heterojunction reached 98.5% yield, and graphene oxide in a (He et al. 2025) helical solar microreactor produced 99.98% biodiesel purity at 200 s residence time with 3% catalyst loading (1:2 oil: methanol molar ratio) (Aghel and Biabani 2024). These results indicate that advanced photocatalyst architectures could enable solar conversion efficiencies above 50%, provided spectral utilisation and geographic variability ($\geq 5\,kWh/m^2$ day of insolation) are addressed through materials such as N-doped TiO_2 or bismuth-based semiconductors (Asahi et al. 2001; Di Valentin et al. 2009; Khan, Farah, et al. 2021; Malato et al. 2002).

From an environmental and process-intensification perspective, photocatalytic transesterification offers several advantages over conventional biodiesel routes. Homogeneous alkaline catalysis, although capable of achieving 95%–98% conversion within 1–2 h, typically requires three to five washing steps and generates large volumes of alkaline wastewater that must be neutralised and treated prior to disposal (Atadashi et al. 2013; Canakci and Sanli 2008; Canakci and Van Gerpen 1999; Demirbas 2009; Freedman et al. 1986; Haas et al. 2006; Ma and Hanna 1999; Radhakrishnan et al. 2007; Vicente et al. 2004). The use of acid as a catalyst imposes even greater environmental concerns, due to higher temperatures, usually above 250°C and requiring about 30% more energy demand than alkaline processes (Kouzu and Hidaka 2012; Lotero et al. 2005; Martín and Grossmann 2012; Semwal et al. 2011; Severson et al. 2013; Yan et al. 2010). In contrast, the photocatalytic route operates under mild thermal conditions (65°C), eliminates neutralisation stages, as required by strong acids and alkalis; produces high-purity glycerol that can be commercialised as a co-product; minimises aqueous waste streams, thereby reducing environmental impact; and allows catalyst recovery and reuse, reducing process costs (Chandhinipriya and Ranjitha 2025; Malato et al. 2002; Welter et al. 2023, 2026; Welter, Santana, et al. 2022). These features position photocatalytic transesterification as a low-waste and low-energy alternative aligned with green-chemistry principles, particularly when integrated with recyclable catalysts and solar photon sources.

Techno-economically, traditional thermal biodiesel processes are a mature and commercial technology, as summarized in Table 10; however, they still rely heavily on raw material costs and are rather energy-consuming during post-treatment. As summarised in Table 9, it can account for up to 80%–88% of the total production cost and energy- and water-intensive during downstream purification. It may represent 60%–80% of the overall process cost. Besides, the feedstock costs in typical alkaline transesterification facilities contribute up to 70%–90% of the total production cost, and other operating expenses (≈US$0.15–0.70 L^{-1}) are related to energy consumption, catalyst loss, purification and wastewater treatment (Atadashi et al. 2011; Bender 1999; Haas et al. 2006). Capital costs are relatively moderate; for example a plant producing 37.8 million L/year was estimated at US$11.3 million, with storage and separation units representing a major amount of the investment (Haas et al. 2006). In contrast, photocatalytic biodiesel routes are still at the developmental stage and associated with higher capital intensity due to specialised photoreactors, optical systems, and light sources. Thus, the estimated cost are about two to three times higher than those of conventional stirred-tank reactors (Duncan 2003; Haas et al. 2006; Malato et al. 2002; Ollis et al. 1991). However, these systems offer the potential for lower operating costs, due to mild operation conditions, reduced energy demand, catalyst reuse, and reduced washing and waste-treatment steps (Duncan 2003; Haas et al. 2006). Techno-economic projections indicate operating costs in the range of US$0.28–0.45 L^{-1} for LED-driven photoreactors and as low as US$0.15–0.25 L^{-1} for solar-driven configurations, suggesting that photocatalytic processes could become economically competitive as reactor costs decrease and scale-up improves (Atadashi et al. 2013; Bender 1999; Duncan 2003; Haas et al. 2006).

Overall, the scale-up to industrial scale of the photocatalytic transesterification will depend on the integration of different parameters, such as photon flux management, multiphase mass transport control, OPEX and CAPEX costs. Although the technology is still at the laboratory stage of development, when combining thin-film or microstructured reactors with catalyst immobilisation, such as TiO_2-coated and solar-driven operation, this approach presents a viable pathway. From a systems perspective, the reduction in downstream purification, catalyst losses, and wastewater generation represents a significant advantage over conventional routes, particularly under increasingly strict environmental regulations. While the capital costs are currently more expensive for photoreactor-based systems, considerable reductions can be expected in operating costs, energy demand, and waste treatment. Hence, prospective scale-up schemes should consider an integrated reactor structure, a continuous-flow arrangement and a solar-compatible photocatalyst to bridge the gap between lab performance and field application.

17571707, 2026, 6, Downloaded from https://onlinelibrary.wiley.com/doi/10.1111/gcbb.70113 by James Cook University, Wiley Online Library on [10/11/2026]. See the Terms and Conditions (https://onlinelibrary.wiley.com/terms-and-conditions) on Wiley Online Library for rules of use; OA articles are governed by the applicable Creative Commons License

TABLE 10 | Comparative techno-economic table: Conventional versus photocatalytic biodiesel.[a]

Sub-item	Conventional route[b]	Photocatalytic route
CAPEX		
Plant construction	US$11.3 million for 37.8 million L/year	Not yet commercial; estimates 2–3× stirred-tank cost
Capital intensity	~US$0.3 per L/year capacity	~US$0.6–1.0 per L/year (projected)
Major cost contributors	Storage tanks (~⅓), reactors, separation units	Photoreactor modules, light sources, optics
Typical capital cost for advanced biofuel plants	~US$2–4.5 per L/year capacity (2nd gen)	Similar or higher for early-stage photoreactors
OPEX		
Feedstock[c]	~US$0.35–0.60/L biodiesel	~US$0.35–0.60/L biodiesel
Energy[d]	US$0.10–0.18/kg FAME	Lower due to mild conditions; projected reduction 30%–60%
Catalyst cost	US$0.08–0.12/kg FAME (non-recoverable base catalysts)	Lower (immobilised or reusable photocatalysts)
Washing and separation	US$0.20–0.30/kg FAME	Reduced due to fewer soap by-products
Waste treatment	US$0.05–0.10/kg FAME	Lower due to reduced wastewater and neutralisation steps
Economic indicators		
Total production cost CAPEX (including feedstock)	~US$0.30–0.70/L (depending on oil)	~US$0.28–0.45/L (LED) ~US$0.15–0.25/L (solar, projected)
Total process OPEX (excluding feedstock)	~US$0.15–0.70/L	~US$0.15–0.45/L (LED) ~US$0.15–0.25/L (solar)
Payback period	3–6 years (typical biodiesel plants)	2.9–5.4 years (pilot catalytic systems; projected for solar-driven photocatalysis)

[a]Acevedo et al. (2015), Atadashi et al. (2011), Bender (1999), Duncan (2003), Gaurav et al. (2013), Haas et al. (2006) and Mustapha et al. (2017).
[b]Catalysts: strong acid (e.g., sulphuric acid)/alkaline (e.g., sodium hydroxide).
[c]Depends on oil source.
[d]Includes, but is not limited to, heating, mixing and separation.

6 | Conclusion

A green transesterification method for converting canola oil to fatty acid methyl esters (FAME) was established using photocatalysis. The process employed a 1:55 M ratio of canola oil to methanol, with 20% TiO_2 ($w_{catalyst}/w_{TGL}$) and UVA irradiation. This approach yielded a 73% (±1.41) conversion at 65°C with vigorous agitation. The photocatalytic reaction involved both triglyceride transesterification and free fatty acid esterification. The catalyst could be recycled by a simple procedure involving only three simple steps (filtration, washing and drying at a mild temperature). The removed organic fraction consisted mainly of reactants and products and can be returned to the process, while the solvent can be recovered by simple distillation, indicating low energy and material demand for catalyst regeneration and minimal addition waste generation. However, its efficiency decreased with each cycle due to accumulation of organic material. When conducted in natural sunlight, the reaction's efficiency dropped significantly to 19% conversion, attributed to the low UVA content and poor photocatalyst absorption in the solar spectrum. Ethanol was tested as a methanol alternative but achieved only 38% conversion due to its lower reactivity. Six kinetic models were applied to the experimental data, with the second-order forward and fourth-order backward reaction model showing the best fit. Thermodynamic properties were also determined, indicating that temperatures above 65°C are preferable for the endothermic reaction and compound miscibility. This developed process avoids common issues in traditional (thermal) homogeneous catalysis, such as extreme temperatures and pH, difficult catalyst handling and reuse, large waste volumes, and complex purifications. However, scaling up heterogeneous photocatalytic processes remains challenging due to significant photon and mass transfer limitations. Future research will explore waste feedstocks with high free fatty acid content, like cooking oil, and investigate scale-up using continuous-flow reactors.

Author Contributions

Rosilene A. Welter: conceptualization, investigation, writing – original draft, methodology, validation, visualization, writing – review and editing. **Osvaldir Pereira Taranto:** conceptualization, funding acquisition, formal analysis, supervision, project administration. **Harrson**

17571707, 2026, 6, Downloaded from https://onlinelibrary.wiley.com/doi/10.1111/gcbb.70113 by James Cook University, Wiley Online Library on [10/11/2026]. See the Terms and Conditions (https://onlinelibrary.wiley.com/terms-and-conditions) on Wiley Online Library for rules of use; OA articles are governed by the applicable Creative Commons License

Santana: conceptualization, validation, visualization, formal analysis, supervision. **Lucimara G. de la Torre:** supervision, revision. **Michael Oelgemöller:** supervision, coordinator, editing.

Acknowledgements

R.A.W. thanks the College of Science and Engineering at James Cook University for financial support (Competitive Research Training Grants 2021 and 2022). The authors thank Assoc.-Prof. George Vamvounis, Dr. Jayson Wau and Dr. Mark Robertson for technical support.

Funding

This work was supported by James Cook University for financial support (Competitive Research Training Grants 2021 and 2022).

Conflicts of Interest

The authors declare no conflicts of interest.

Data Availability Statement

The datasets generated during this study are available in the Zenodo repository (https://doi.org/10.5281/zenodo.19059262).

References

Abdelkhalik, A., H. Elsayed, M. Hassan, M. Nour, A. B. Shehata, and M. Helmy. 2018. "Using Thermal Analysis Techniques for Identifying the Flash Point Temperatures of Some Lubricant and Base Oils." *Egyptian Journal of Petroleum* 27, no. 1: 131–136. https://doi.org/10.1016/j.ejpe.2017.02.006.

Acevedo, J. C., J. A. Hernández, C. F. Valdés, and S. K. Khanal. 2015. "Analysis of Operating Costs for Producing Biodiesel From Palm Oil at Pilot-Scale in Colombia." *Bioresource Technology* 188: 117–123. https://doi.org/10.1016/j.biortech.2015.01.071.

Aghel, B., and A. Biabani. 2024. "Using Solar Microreactors and Photocatalysts to Synthesize Biodiesel." *Renewable Energy* 220: 119654. https://doi.org/10.1016/j.renene.2023.119654.

Alsharifi, M., H. Znad, S. Hena, and M. Ang. 2017. "Biodiesel Production From Canola Oil Using Novel Li/TiO_2 as a Heterogeneous Catalyst Prepared via Impregnation Method." *Renewable Energy* 114: 1077–1089. https://doi.org/10.1016/j.renene.2017.07.117.

Andrade, R. D. A., E. Pozzebom, E. A. Faria, F. D. Filho, P. A. Z. Suarez, and A. G. S. do Prado. 2011. "Thermal Behavior of Diesel/Biodiesel Blends of Biodiesel Obtained From Buriti Oil." *Acta Scientiarum. Technology* 34, no. 2: 243–250. https://doi.org/10.4025/actascitechnol.v34i2.12797.

Ansari, S. A., M. M. Khan, M. O. Ansari, and M. H. Cho. 2016. "Nitrogen-Doped Titanium Dioxide (N-Doped TiO_2) for Visible Light Photocatalysis." *New Journal of Chemistry* 40, no. 4: 3000–3009. https://doi.org/10.1039/c5nj03478g.

ARPANSA. 2022. *Ultraviolet Radiation Monitoring: UV Index*. Australian Radiation Protection and Nuclear Safety Agency. https://www.arpansa.gov.au/our-services/monitoring/ultraviolet-radiation-monitoring/ultraviolet-radiation-index.

Arunachalam, A., S. Dhanapandian, C. Manoharan, and G. Sivakumar. 2015. "Physical Properties of Zn-Doped TiO_2 Thin Films With Spray Pyrolysis Technique and Its Effects in Antibacterial Activity." *Spectrochimica Acta Part A: Molecular and Biomolecular Spectroscopy* 138: 105–112. https://doi.org/10.1016/j.saa.2014.11.016.

Arzamendi, G., I. Campo, E. Arguiñarena, M. Sánchez, M. Montes, and L. M. Gandía. 2007. "Synthesis of Biodiesel With Heterogeneous NaOH/Alumina Catalysts: Comparison With Homogeneous NaOH." *Chemical Engineering Journal* 134, no. 1–3: 123–130. https://doi.org/10.1016/j.cej.2007.03.049.

Asahi, R., T. Morikawa, T. Ohwaki, K. Aoki, and Y. Taga. 2001. "Visible-Light Photocatalysis in Nitrogen-Doped Titanium Oxides." *Science* 293, no. 5528: 269–271. https://doi.org/10.1126/science.1061051.

ASTM International. 2015. *ASTM D6751-15: Standard Specification for Biodiesel Fuel Blend Stock (B100) for Middle Distillate Fuels*. ASTM International.

ASTM International. 2016. *ASTM D7398: Standard Test Method for Determination of Flash Point by Small Scale Closed Cup Tester*. ASTM International.

ASTM International. 2017a. *ASTM D98: Standard Test Method for Pour Point of Petroleum Products*. ASTM International.

ASTM International. 2017c. *ASTM D6584: Standard Test Method for Determination of Free and Total Glycerin in Biodiesel Methyl Esters by Gas Chromatography*. ASTM International.

ASTM International. 2018. *ASTM D93: Standard Test Methods for Flash Point by Pensky–Martens Closed Cup Tester*. ASTM International.

Atadashi, I. M., M. K. Aroua, A. R. Abdul Aziz, and N. M. N. Sulaiman. 2013. "The Effects of Catalysts in Biodiesel Production: A Review." *Journal of Industrial and Engineering Chemistry* 19, no. 1: 14–26. https://doi.org/10.1016/j.jiec.2012.07.009.

Atadashi, I. M., M. K. Aroua, and A. A. Aziz. 2011. "Biodiesel Separation and Purification: A Review." *Renewable Energy* 36, no. 2: 437–443. https://doi.org/10.1016/j.renene.2010.07.019.

Ayadi, M., F. N. A. Saragih, S. Awad, et al. 2021. "Two-Step Methanolysis and Ethanolysis of Olive Pomace Oil Using Olive-Pomace-Based Heterogeneous Acid Catalyst." *Fuel* 296: 120678. https://doi.org/10.1016/j.fuel.2021.120678.

Bahnemann, D. 2004. "Photocatalytic Water Treatment: Solar Energy Applications." *Solar Energy* 77, no. 5: 445–459. https://doi.org/10.1016/j.solener.2004.03.031.

Bender, M. 1999. "Economic Feasibility Review for Community-Scale Farmer Cooperatives for Biodiesel." *Bioresource Technology* 70, no. 1: 81–87. https://doi.org/10.1016/S0960-8524(99)00009-7.

Berrebi, G., P. Dufresne, and Y. Jacquier. 1994. "Recycling of Spent Hydroprocessing Catalysts: EURECAT Technology." *Resources, Conservation and Recycling* 10, no. 1–2: 1–9. https://doi.org/10.1016/0921-3449(94)90032-9.

Boocock, D. G. B., S. K. Konar, V. Mao, and H. Sidi. 1996. "Fast One-Phase Oil-Rich Processes for the Preparation of Vegetable Oil Methyl Esters." *Biomass and Bioenergy* 11, no. 1: 43–50. https://doi.org/10.1016/0961-9534(95)00111-5.

Borah, M. J., A. Devi, R. A. Saikia, and D. Deka. 2018. "Biodiesel Production From Waste Cooking Oil Catalyzed by In-Situ Decorated TiO_2 on Reduced Graphene Oxide Nanocomposite." *Energy* 158: 881–889. https://doi.org/10.1016/j.energy.2018.06.079.

Braham, R. J., and A. T. Harris. 2009. "Review of Major Design and Scale-Up Considerations for Solar Photocatalytic Reactors." *Industrial & Engineering Chemistry Research* 48, no. 19: 8890–8905. https://doi.org/10.1021/ie900859z.

Brahim, I. O., M. Belmedani, H. Hadoun, and A. Belgacem. 2021. "The Photocatalytic Degradation Kinetics of Food Dye in Aqueous Solution Under UV/ZnO System." *Reaction Kinetics, Mechanisms and Catalysis* 133, no. 2: 1075–1095. https://doi.org/10.1007/s11144-021-02006-8.

Byrne, J. A., B. R. Eggins, N. M. D. Brown, B. McKinney, and M. Rouse. 1998. "Immobilisation of TiO_2 Powder for the Treatment of Polluted

17571707, 2026, 6, Downloaded from https://onlinelibrary.wiley.com/doi/10.1111/gcbb.70113 by James Cook University, Wiley Online Library on [10/11/2026]. See the Terms and Conditions (https://onlinelibrary.wiley.com/terms-and-conditions) on Wiley Online Library for rules of use; OA articles are governed by the applicable Creative Commons License

Water." *Applied Catalysis B: Environmental* 17, no. 1–2: 25–36. https://doi.org/10.1016/S0926-3373(97)00101-X.

Caballero, B., ed. 2003. *Encyclopedia of Food Sciences and Nutrition*. 2nd ed. Academic Press.

Cai, J., and L. Bi. 2008. "Precision of the Coats and Redfern Method for the Determination of the Activation Energy Without Neglecting the Low-Temperature End of the Temperature Integral." *Energy & Fuels* 22, no. 4: 2172–2174. https://doi.org/10.1021/ef8002125.

Calero, J., D. Luna, E. D. Sancho, et al. 2014. "Development of a New Biodiesel That Integrates Glycerol, by Using CaO as Heterogeneous Catalyst, in the Partial Methanolysis of Sunflower Oil." *Fuel* 122: 94–102. https://doi.org/10.1016/j.fuel.2014.01.033.

Cambié, D., F. Zhao, V. Hessel, M. G. Debije, and T. Noël. 2017. "A Leaf-Inspired Luminescent Solar Concentrator for Energy-Efficient Continuous-Flow Photochemistry." *Angewandte Chemie International Edition* 56, no. 4: 1050–1054. https://doi.org/10.1002/anie.201611101.

Canakci, M., and H. Sanli. 2008. "Biodiesel Production From Various Feedstocks and Their Effects on the Fuel Properties." *Journal of Industrial Microbiology & Biotechnology* 35, no. 5: 431–441. https://doi.org/10.1007/s10295-008-0337-6.

Canakci, M., and J. Van Gerpen. 1999. "Biodiesel Production via Acid Catalysis." *Transactions of ASAE* 42, no. 5: 1203–1210.

Carp, O., C. L. Huisman, and A. Reller. 2004. "Photoinduced Reactivity of Titanium Dioxide." *Progress in Solid State Chemistry* 32, no. 1–2: 33–177. https://doi.org/10.1016/j.progsolidstchem.2004.08.001.

Cassano, A. E., and O. M. Alfano. 2000. "Reaction Engineering of Suspended Solid Heterogeneous Photocatalytic Reactors." *Catalysis Today* 58, no. 2–3: 167–197. https://doi.org/10.1016/S0920-5861(00)00251-0.

Chaemchuen, S., P. M. Heynderickx, and F. Verpoort. 2020. "Kinetic Modelling of Oleic Acid Esterification With UiO-66: From Intrinsic Experimental Data to Kinetics via Elementary Reaction Steps." *Chemical Engineering Journal* 394: 124816. https://doi.org/10.1016/j.cej.2020.124816.

Chandhinipriya, S., and J. Ranjitha. 2025. "Visible-Light-Driven Photocatalytic Synthesis of Methyl Oleate Using TiO_2/Fe_2O_3 With Process Optimization and Scale-Up: A Path Toward a Drop-In Sustainable Fuel Approach." *Results in Chemistry* 16: 102510. https://doi.org/10.1016/j.rechem.2025.102510.

Chen, X., Z. Li, Y. Chun, F. Yang, H. Xu, and X. Wu. 2020. "Effect of the Formation of Diglycerides/Monoglycerides on the Kinetic Curve in Oil Transesterification With Methanol Catalyzed by Calcium Oxide." *ACS Omega* 5, no. 9: 4646–4656. https://doi.org/10.1021/acsomega.9b04431.

Choo, K. H. 2018. "Modeling Photocatalytic Membrane Reactors." In *Current Trends and Future Developments on (Bio-)Membranes: Photocatalytic Membranes and Photocatalytic Membrane Reactors*, vol. 1, 297–316. Elsevier. https://doi.org/10.1016/B978-0-12-813549-5.00010-4.

Chouhan, A. P. S., and A. K. Sarma. 2011. "Modern Heterogeneous Catalysts for Biodiesel Production: A Comprehensive Review." *Renewable and Sustainable Energy Reviews* 15, no. 9: 4378–4399. https://doi.org/10.1016/j.rser.2011.07.112.

Colucci, J. A., E. E. Borrero, and F. Alape. 2005. "Biodiesel From an Alkaline Transesterification Reaction of Soybean Oil Using Ultrasonic Mixing." *Journal of the American Oil Chemists' Society* 82, no. 7: 525–530. https://doi.org/10.1007/s11746-005-1104-3.

Corro, G., Y. Paniagua, U. Pal, F. Bañuelos, and M. Rosas. 2013. "Generation of Biodiesel From *Jatropha curcas* Oil Using Supported Iron Oxide Catalysts." *Applied Catalysis A: General* 452: 1–8. https://doi.org/10.1016/j.apcata.2012.11.015.

De, A., and S. S. Boxi. 2020. "Application of cu-Impregnated TiO_2 as a Heterogeneous Nanocatalyst for the Production of Biodiesel From Palm Oil." *Fuel* 265: 117019. https://doi.org/10.1016/j.fuel.2020.117019.

Demirbas, A. 2009. "Progress and Recent Trends in Biodiesel Fuels." *Energy Conversion and Management* 50, no. 1: 14–34. https://doi.org/10.1016/j.enconman.2008.09.001.

Di Valentin, C., G. Pacchioni, and A. Selloni. 2009. "Reduced and n-Type Doped TiO_2: Nature of Ti^{3+} Species." *Journal of Physical Chemistry C* 113, no. 48: 20543–20552. https://doi.org/10.1021/jp9061797.

dos Passos, R. M., R. S. B. Ferreira, M. A. Morgano, et al. 2024. "Ethyl Biodiesel Production From Crude Soybean Oil Using Enzymatic Degumming–Transesterification Associated Process." *Industrial Crops and Products* 222: 119930. https://doi.org/10.1016/j.indcrop.2024.119930.

Du, J., R. K. Yuan, R. X. Hu, H. L. Zhang, Y. T. Qi, and W. N. Zhang. 2022. "Biodiesel Production From *Momordica cochinchinensis* (Lour.) Spreng Seed Oil." *Fuel* 314: 123047. https://doi.org/10.1016/j.fuel.2021.123047.

Duncan, J. 2003. *Costs of Biodiesel Production*. Energy Efficiency and Conservation Authority.

Encinar, J., A. Pardal, N. Sánchez, and S. Nogales. 2018. "Biodiesel by Transesterification of Rapeseed Oil Using Ultrasound: A Kinetic Study of Base-Catalyzed Reactions." *Energies* 11, no. 9: 2229. https://doi.org/10.3390/en11092229.

Encinar, J. M., J. F. González, and A. Rodríguez-Reinares. 2007. "Ethanolysis of Used Frying Oil: Biodiesel Preparation and Characterization." *Fuel Processing Technology* 88, no. 5: 513–522. https://doi.org/10.1016/j.fuproc.2007.01.002.

European Committee for Standardization, EC. 2003. *En 14104: Fat and Oil Derivatives – Fatty Acid Methyl Esters (FAME) – Determination of Acid Value*. European Standard.

Ezzati, R. 2018. "Kinetics and Thermodynamics of the Esterification Reaction According to the Langmuir–Hinshelwood Mechanism." *Iranian Journal of Catalysis* 8: 41–46.

Ferrão-Gonzales, A. D., I. C. Véras, F. A. L. Silva, H. M. Alvarez, and V. H. Moreau. 2011. "Thermodynamic Analysis of the Kinetics Reactions of the Production of FAME and FAEE Using Novozyme 435 as Catalyst." *Fuel Processing Technology* 92, no. 5: 1007–1011. https://doi.org/10.1016/j.fuproc.2010.12.023.

Freedman, B., R. O. Butterfield, and E. H. Pryde. 1986. "Transesterification Kinetics of Soybean Oil." *Journal of the American Oil Chemists' Society* 63, no. 10: 1375–1380. https://doi.org/10.1007/BF02679606.

Freedman, B., E. H. Pryde, and T. L. Mounts. 1984. "Variables Affecting the Yields of Fatty Esters From Transesterified Vegetable Oils." *Journal of the American Oil Chemists' Society* 61, no. 10: 1638–1643. https://doi.org/10.1007/BF02541649.

Fujishima, A., X. Zhang, and D. A. Tryk. 2008. "TiO_2 Photocatalysis and Related Surface Phenomena." *Surface Science Reports* 63, no. 12: 515–582. https://doi.org/10.1016/j.surfrep.2008.10.001.

Gadore, V., S. R. Mishra, and M. Ahmaruzzaman. 2025. "SnS_2/ZIF-67 Nanocomposite: A Novel Bifunctional, Highly Efficient, and Reusable Photocatalyst for Enhanced Visible-Light-Assisted Biodiesel Production and Degradation of Tinidazole." *Materials Research Bulletin* 183: 113177. https://doi.org/10.1016/j.materresbull.2024.113177.

Galvan, D., L. M. de Aguiar, J. J. R. Rohwedder, D. Borsato, and M. H. M. Killner. 2020. "Online Monitoring of Transesterification Reaction by Medium-Resolution Benchtop ^{1}H-NMR and NIR Spectroscopy." *Fuel Processing Technology* 208: 106511. https://doi.org/10.1016/j.fuproc.2020.106511.

Gardy, J., A. Hassanpour, X. Lai, M. H. Ahmed, and M. Rehan. 2017. "Biodiesel Production From Used Cooking Oil Using a Novel Surface-Functionalized TiO_2 Nano-Catalyst." *Applied Catalysis B: Environmental* 207: 297–310. https://doi.org/10.1016/j.apcatb.2017.01.080.

17571707, 2026, 6, Downloaded from https://onlinelibrary.wiley.com/doi/10.1111/gcbb.70113 by James Cook University, Wiley Online Library on [10/11/2026]. See the Terms and Conditions (https://onlinelibrary.wiley.com/terms-and-conditions) on Wiley Online Library for rules of use; OA articles are governed by the applicable Creative Commons License

Gaurav, A., S. Dumas, C. T. Q. Mai, and F. T. T. Ng. 2019. "A Kinetic Model for a Single-Step Biodiesel Production From a High Free Fatty Acid Feedstock Over a Solid Heteropolyacid Catalyst." *Green Energy & Environment* 4, no. 3: 328–341. https://doi.org/10.1016/j.gee.2019.03.004.

Gaurav, A., M. L. Leite, F. T. T. Ng, and G. L. Rempel. 2013. "Transesterification of Triglyceride to Fatty Acid Alkyl Esters (Biodiesel): Comparison of Utility Requirements and Capital Costs Between Reaction–Separation and Catalytic Distillation Configurations." *Energy & Fuels* 27, no. 11: 6847–6857. https://doi.org/10.1021/ef401790n.

Gelbard, G., O. Brès, R. M. Vargas, R. Vielfaure, and U. F. Schuchardt. 1995. "^{1}H Nuclear Magnetic Resonance Determination of the Yield of the Transesterification of Rapeseed Oil With Methanol." *Journal of the American Oil Chemists' Society* 72, no. 10: 1239–1241. https://doi.org/10.1007/BF02540998.

Ghani, N., J. Iqbal, S. Sadaf, H. N. Bhatti, and M. Asgher. 2020. "Comparison of Photo-Esterification Capability of Bismuth Vanadate With Reduced Graphene Oxide/Bismuth Vanadate Composite for Biodiesel Production From High Free Fatty Acid Non-Edible Oil." *ChemistrySelect* 5, no. 29: 9245–9253. https://doi.org/10.1002/slct.202001913.

Granados, M. L., M. D. Z. Poves, D. M. Alonso, et al. 2007. "Biodiesel From Sunflower Oil by Using Activated Calcium Oxide." *Applied Catalysis B: Environmental* 73, no. 3: 317–326. https://doi.org/10.1016/j.apcatb.2006.12.017.

Guo, M., W. Jiang, C. Chen, et al. 2021. "Process Optimization of Biodiesel Production From Waste Cooking Oil by Esterification of Free Fatty Acids Using La^{3+}/ZnO–TiO_2 Photocatalyst." *Energy Conversion and Management* 229: 113745. https://doi.org/10.1016/j.enconman.2020.113745.

Guo, M., W. Jiang, J. Ding, and J. Lu. 2022. "Highly Active and Recyclable CuO/ZnO as Photocatalyst for Transesterification of Waste Cooking Oil to Biodiesel and Kinetics Study." *Fuel* 315: 123254. https://doi.org/10.1016/j.fuel.2022.123254.

Haas, M. J., A. J. McAloon, W. C. Yee, and T. A. Foglia. 2006. "A Process Model to Estimate Biodiesel Production Costs." *Bioresource Technology* 97, no. 4: 671–678. https://doi.org/10.1016/j.biortech.2005.03.039.

He, L., L. L. Zhang, H. Zhou, et al. 2025. "Boosting Photocatalytic Upcycling of Liquid Biomass Into Biodiesel via Microenvironment Modulation." *Advanced Energy Materials* 15, no. 5: 2403168. https://doi.org/10.1002/aenm.202403168.

Herrmann, J. M. 2010. "Photocatalysis Fundamentals Revisited to Avoid Several Misconceptions." *Applied Catalysis B: Environmental* 99, no. 3–4: 461–468. https://doi.org/10.1016/j.apcatb.2010.05.012.

Hoffmann, N. 2015. "Photocatalysis With TiO_2 Applied to Organic Synthesis." *Australian Journal of Chemistry* 68, no. 11: 1621–1631. https://doi.org/10.1071/CH15322.

Islam, A., S. H. Teo, M. T. Islam, et al. 2025. "Harnessing Visible Light for Sustainable Biodiesel Production With Ni/Si/MgO Photocatalyst." *Renewable and Sustainable Energy Reviews* 208: 115033. https://doi.org/10.1016/j.rser.2024.115033.

Jaiswal, S. K., N. T. Prakash, and R. Prakash. 2016. "^{1}H NMR-Based Quantification of Ethyl Ester in Biodiesel: A Comparative Study of Product-Dependent Derivations." *Analytical Chemistry Letters* 6, no. 5: 518–525. https://doi.org/10.1080/22297928.2016.1246977.

Kanakaraju, D., B. D. Glass, and M. Oelgemöller. 2014. "Titanium Dioxide Photocatalysis for Pharmaceutical Wastewater Treatment." *Environmental Chemistry Letters* 12: 27–47. https://doi.org/10.1007/s10311-013-0428-0.

Kanakaraju, D., C. A. Motti, B. D. Glass, and M. Oelgemöller. 2016. "Solar Photolysis Versus TiO_2-Mediated Solar Photocatalysis: A Kinetic Study of the Degradation of Naproxen and Diclofenac in Various Water Matrices." *Environmental Science and Pollution Research* 23, no. 17: 17437–17448. https://doi.org/10.1007/s11356-016-6906-8.

Kar, R., O. Gupta, K. Mandol, and S. Bhattacharjee. 2012. "Performance Study on Photocatalysis of Phenol Solution in a UV-Irradiated Reactor." *Journal of Chemical Engineering & Process Technology* 4, no. 1: 1000143. https://doi.org/10.4172/2157-7048.1000143.

Karan, P., P. Mukhopadhyay, and R. Chakraborty. 2020. "Quartz Halogen–Ultrasonication Integrated Rotating Reactor for Efficient Photocatalytic–Thermocatalytic Synthesis of Glyceryl Monocaprin: Kinetics of Heterogeneous Esterification." *Asia-Pacific Journal of Chemical Engineering* 15, no. 1: e2379. https://doi.org/10.1002/apj.2379.

Khaligh, N. G., T. Mihankhah, Z. Shahnavaz, L. Zaharani, and M. R. Johan. 2021. "Solar Energy and TiO_2 Nanotubes: Biodiesel Production From Waste Cooking Olive Oil." *Environmental Progress & Sustainable Energy* 40, no. 2: e13537. https://doi.org/10.1002/ep.13537.

Khan, M., H. Farah, N. Iqbal, T. Noor, M. Z. B. Amjad, and S. S. E. Bukhari. 2021. "A TiO_2 Composite With Graphitic Carbon Nitride as a Photocatalyst for Biodiesel Production From Waste Cooking Oil." *RSC Advances* 11, no. 59: 37575–37583. https://doi.org/10.1039/D1RA07796A.

Khan, N., S. H. Park, L. Kadima, et al. 2021. "Locally Sustainable Biodiesel Production From Waste Cooking Oil and Grease Using a Deep Eutectic Solvent: Characterization, Thermal Properties, and Blend Performance." *ACS Omega* 6, no. 13: 9204–9212. https://doi.org/10.1021/acsomega.1c00556.

Khezrianjoo, S., and H. D. Revanasiddappa. 2012. "Langmuir–Hinshelwood Kinetic Expression for the Photocatalytic Degradation of Metanil Yellow Aqueous Solutions by ZnO Catalyst." *Chemical Sciences Journal* 2012: CSJ-85.

Kim, D.-S., M. Hanifzadeh, and A. Kumar. 2018. "Trend of Biodiesel Feedstock and Its Impact on Biodiesel Emission Characteristics." *Environmental Progress & Sustainable Energy* 37, no. 1: 7–19. https://doi.org/10.1002/ep.12800.

Kipcak, A. S., F. T. Senberber, E. M. Derun, N. Tugrul, and S. Piskin. 2015. "Characterization and Thermal Dehydration Kinetics of Zinc Borates Synthesized From Zinc Sulfate and Zinc Chloride." *Research on Chemical Intermediates* 41, no. 11: 9129–9143. https://doi.org/10.1007/s11164-015-1952-2.

Kivevele, T. T., M. M. Mbarawa, A. Bereczky, T. Laza, and J. Madarasz. 2011. "Impact of Antioxidant Additives on the Oxidation Stability of Biodiesel Produced From *Croton megalocarpus* Oil." *Fuel Processing Technology* 92, no. 6: 1244–1248. https://doi.org/10.1016/j.fuproc.2011.02.009.

Konstantinou, I. K., and T. A. Albanis. 2003. "Photocatalytic Transformation of Pesticides in Aqueous Titanium Dioxide Suspensions Using Artificial and Solar Light: Intermediates and Degradation Pathways." *Applied Catalysis B: Environmental* 42, no. 4: 319–335. https://doi.org/10.1016/S0926-3373(02)00266-7.

Kouzu, M., and J. S. Hidaka. 2012. "Transesterification of Vegetable Oil Into Biodiesel Catalyzed by CaO: A Review." *Fuel* 93: 1–12. https://doi.org/10.1016/j.fuel.2011.09.015.

Kulak, A. I., and D. A. Kiiliomin. 2018. "Double Bond System Formation in the Process of Thermocatalytic Dehydration of Polyvinyl Alcohol." *Doklady of the National Academy of Sciences of Belarus* 62, no. 5: 569–575. https://doi.org/10.29235/1561-8323-2018-62-5-569-575.

Lai, Y., B. Wang, X. Chen, et al. 2014. "Thermogravimetric Analysis of Combustion Characteristics of Palm Oil and Rapeseed Oil Biodiesel." *Biotechnology* 14, no. 1: 9–15. https://doi.org/10.3923/biotech.2015.9.15.

Leung, D. Y. C., X. Wu, and M. K. H. Leung. 2010. "A Review on Biodiesel Production Using Catalyzed Transesterification." *Applied Energy* 87, no. 4: 1083–1095. https://doi.org/10.1016/j.apenergy.2009.10.006.

Li, K., C. Teng, S. Wang, and Q. Min. 2021. "Recent Advances in TiO_2-Based Heterojunctions for Photocatalytic CO_2 Reduction With Water

17571707, 2026, 6, Downloaded from https://onlinelibrary.wiley.com/doi/10.1111/gcbb.70113 by James Cook University, Wiley Online Library on [10/11/2026]. See the Terms and Conditions (https://onlinelibrary.wiley.com/terms-and-conditions) on Wiley Online Library for rules of use; OA articles are governed by the applicable Creative Commons License

Oxidation: A Review." *Frontiers in Chemistry* 9: 637501. https://doi.org/10.3389/fchem.2021.637501.

Lotero, E., Y. Liu, D. E. Lopez, K. Suwannakarn, D. A. Bruce, and J. G. Goodwin. 2005. "Synthesis of Biodiesel via Acid Catalysis." *Industrial & Engineering Chemistry Research* 44, no. 14: 5353–5363. https://doi.org/10.1021/ie049157g.

Lu, J. J., and W. H. Chen. 2015. "Investigation on the Ignition and Burnout Temperatures of Bamboo and Sugarcane Bagasse by Thermogravimetric Analysis." *Applied Energy* 160: 49–57. https://doi.org/10.1016/j.apenergy.2015.09.026.

Lukić, I., Ž. Kesić, S. Maksimović, et al. 2013. "Kinetics of Sunflower and Used Vegetable Oil Methanolysis Catalyzed by CaO·ZnO." *Fuel* 113: 367–378. https://doi.org/10.1016/j.fuel.2013.05.093.

Ma, F., and M. A. Hanna. 1999. "Biodiesel Production: A Review." *Bioresource Technology* 70, no. 1: 1–15. https://doi.org/10.1016/S0960-8524(99)00025-5.

Makuła, P., M. Pacia, and W. Macyk. 2018. "How to Correctly Determine the Band Gap Energy of Modified Semiconductor Photocatalysts Based on UV–Vis Spectra." *Journal of Physical Chemistry Letters* 9, no. 23: 6814–6817. https://doi.org/10.1021/acs.jpclett.8b02892.

Malato, S., J. Blanco, A. Vidal, and C. Richter. 2002. "Photocatalysis With Solar Energy at a Pilot-Plant Scale: An Overview." *Applied Catalysis B: Environmental* 37, no. 1: 1–15. https://doi.org/10.1016/S0926-3373(01)00315-0.

Manique, M. C., A. P. Silva, A. K. Alves, and C. P. Bergmann. 2016. "Application of Hydrothermally Produced TiO_2 Nanotubes in Photocatalytic Esterification of Oleic Acid." *Materials Science and Engineering B* 206: 17–21. https://doi.org/10.1016/j.mseb.2016.01.001.

Martín, M., and I. E. Grossmann. 2012. "On the Systematic Synthesis of Sustainable Biorefineries." *Industrial & Engineering Chemistry Research* 52, no. 9: 3044–3064. https://doi.org/10.1021/ie2030213.

Mataghare, B. C., V. S. Patil, P. R. Yadav, et al. 2024. "Novel Porphyrin Photocatalyst Intertwined With Ionic Liquid and Sulfonic Acid Groups for Facile Photo-Transesterification of Used Frying Oil." *Fuel* 373: 132295. https://doi.org/10.1016/j.fuel.2024.132295.

McCurry, J. D. 2012. *GC Analysis of Total Fatty Acid Methyl Esters (FAME) and Methyl Linolenate in Biodiesel Using the Revised EN14103:2011 Method* (Application Note 5991-0441EN). Agilent Technologies, Inc.

Micic, O. I., Y. Zhang, K. R. Cromack, A. D. Trifunac, and M. C. Thurnauer. 1993. "Trapped Holes on Titania Colloids Studied by Electron Paramagnetic Resonance." *Journal of Physical Chemistry* 97, no. 28: 7277–7283. https://doi.org/10.1021/j100130a026.

Mihankhah, T., M. Delnavaz, and N. G. Khaligh. 2018. "Application of TiO_2 Nanoparticles for Eco-Friendly Biodiesel Production From Waste Olive Oil." *International Journal of Green Energy* 15, no. 2: 69–75. https://doi.org/10.1080/15435075.2018.1423975.

Mofijur, M., M. G. Rasul, N. M. S. Hassan, H. H. Masjuki, M. A. Kalam, and H. M. Mahmudul. 2017. "Assessment of Physical, Chemical, and Tribological Properties of Different Biodiesel Fuels." In *Clean Energy for Sustainable Development*, edited by G. R. Mohammad, A. K. Azad, and C. S. Subhash, vol. 1, 1st ed., 441–463. Academic Press. https://doi.org/10.1016/B978-0-12-805423-9.00014-4.

Mostafa, S. S. M., and N. S. El-Gendy. 2017. "Evaluation of Fuel Properties for Microalgae *Spirulina platensis* Biodiesel and Its Blends With Egyptian Petro-Diesel." *Arabian Journal of Chemistry* 10: S2040–S2050. https://doi.org/10.1016/j.arabjc.2013.07.034.

Mueses, M. A., F. Machuca-Martinez, and G. Li Puma. 2013. "Effective Quantum Yield and Reaction Rate Model for Evaluation of Photocatalytic Degradation of Water Contaminants in Heterogeneous Pilot-Scale Solar Photoreactors." *Chemical Engineering Journal* 215–216: 937–947. https://doi.org/10.1016/j.cej.2012.11.076.

Mustapha, W. F., T. F. Bolkesjø, T. Martinsen, and E. Trømborg. 2017. "Techno-Economic Comparison of Promising Biofuel Conversion Pathways in a Nordic Context—Effects of Feedstock Costs and Technology Learning." *Energy Conversion and Management* 149: 368–380. https://doi.org/10.1016/j.enconman.2017.07.004.

Nagrale, P. 2024. *Biodiesel Market: Size, Share & Growth Analysis Report by Application, Type, and Region—Trends & Industry Forecast to 2035* (Report ID: MRFR/EnP/0992-HCR). Market Research Future. https://www.marketresearchfuture.com/reports/biodiesel-market-1521.

Nicolau, C., A. Klein, C. Silva, et al. 2018. "Thermal Properties of Blends of Methyl and Ethyl Esters Prepared From Babassu and Soybean Oils." *Journal of the Brazilian Chemical Society* 29, no. 8: 1672–1679. https://doi.org/10.21577/0103-5053.20180040.

Nieva-Echevarría, B., E. Goicoechea, M. J. Manzanos, and M. D. Guillén. 2015. "Usefulness of ^{1}H NMR in Assessing the Extent of Lipid Digestion." *Food Chemistry* 179: 182–190. https://doi.org/10.1016/j.foodchem.2015.01.104.

Noureddini, H., and D. Zhu. 1997. "Kinetics of Transesterification of Soybean Oil." *Journal of the American Oil Chemists' Society* 74, no. 11: 1457–1463. https://doi.org/10.1007/s11746-997-0254-2.

Oelgemöller, M. 2012. "Highlights of Photochemical Reactions in Microflow Reactors." *Chemical Engineering & Technology* 35, no. 7: 1144–1152. https://doi.org/10.1002/ceat.201200009.

Oelgemöller, M. 2016. "Solar Photochemical Synthesis: From the Beginnings of Organic Photochemistry to the Solar Manufacturing of Commodity Chemicals." *Chemical Reviews* 116, no. 17: 9664–9682. https://doi.org/10.1021/acs.chemrev.5b00720.

Ogunkunle, O., and N. A. Ahmed. 2019. "A Review of Global Current Scenario of Biodiesel Adoption and Combustion in Vehicular Diesel Engines." *Energy Reports* 5: 1560–1579. https://doi.org/10.1016/j.egyr.2019.10.028.

Ohtani, B. 2011. "Photocatalysis by Inorganic Solid Materials: Revisiting Its Definition, Concepts, and Experimental Procedures." In *Advances in Inorganic Chemistry*, edited by R. van Eldik and C. D. Hubbard, vol. 63, 395–430. Academic Press. https://doi.org/10.1016/B978-0-12-385904-4.00001-9.

Ollis, D. F., E. Pelizzetti, and N. Serpone. 1991. "Photocatalyzed Destruction of Water Contaminants." *Environmental Science & Technology* 25, no. 9: 1522–1529. https://doi.org/10.1021/es00021a001.

Omar, W. N. N. W., and N. A. S. Amin. 2011. "Biodiesel Production From Waste Cooking Oil Over Alkaline-Modified Zirconia Catalyst." *Fuel Processing Technology* 92, no. 12: 2397–2405. https://doi.org/10.1016/j.fuproc.2011.08.009.

Onu, P., and C. Mbohwa. 2021. "New Approach and Prospects of Agrowaste Resources Conversion for Energy Systems Performance and Development." In *Agricultural Waste Diversity and Sustainability Issues*, edited by S. S. Muthu, 97–118. Elsevier. https://doi.org/10.1016/B978-0-323-85402-3.00007-3.

Oyekunle, D. T., M. Barasa, E. A. Gendy, and S. K. Tiong. 2023. "Heterogeneous Catalytic Transesterification for Biodiesel Production: Feedstock Properties, Catalysts, and Process Parameters." *Process Safety and Environmental Protection* 177: 844–867. https://doi.org/10.1016/j.psep.2023.07.064.

Özyiğit, B., E. Sayilganlar, and E. Akbay. 2024. "Photocatalytic Esterification of Acetic Acid With Methanol Over Metal-Exchanged Phosphotungstate." *Journal of Photochemistry and Photobiology A: Chemistry* 447: 115280. https://doi.org/10.1016/j.jphotochem.2023.115280.

Pandey, S. 2024. *Aviation, Maritime Demand to Fuel Global Biofuel Feedstock Race by 2030*. S&P Global Commodity Insights. https://www.spglobal.com/commodityinsights/en/market-insights/latest-news/agriculture/100924-aviation-maritime-demand-to-fuel-global-biofuel-feedstock-race-by-2030.

17571707, 2026, 6, Downloaded from https://onlinelibrary.wiley.com/doi/10.1111/gcbb.70113 by James Cook University, Wiley Online Library on [10/11/2026]. See the Terms and Conditions (https://onlinelibrary.wiley.com/terms-and-conditions) on Wiley Online Library for rules of use; OA articles are governed by the applicable Creative Commons License

Pawar, M., S. T. Sendoğdular, and P. Gouma. 2018. "A Brief Overview of TiO_2 Photocatalyst for Organic Dye Remediation: Case Study of Reaction Mechanisms Involved in Ce–TiO_2 Photocatalysts System." *Journal of Nanomaterials* 2018: 1–13. https://doi.org/10.1155/2018/5953609.

Pelaez, M., N. T. Nolan, S. C. Pillai, et al. 2012. "A Review on the Visible Light Active Titanium Dioxide Photocatalysts for Environmental Applications." *Applied Catalysis B: Environmental* 125: 331–349. https://doi.org/10.1016/j.apcatb.2012.05.036.

Pereira, C. O., M. F. Portilho, C. A. Henriques, and F. M. Z. Zotin. 2014. "$SnSO_4$ as Catalyst for Simultaneous Transesterification and Esterification of Acid Soybean Oil." *Journal of the Brazilian Chemical Society* 25: 2409–2416. https://doi.org/10.5935/0103-5053.20140267.

Pérez, M. H., G. Peñuela, M. I. Maldonado, et al. 2006. "Degradation of Pesticides in Water Using Solar Advanced Oxidation Processes." *Applied Catalysis B: Environmental* 64, no. 3–4: 272–281. https://doi.org/10.1016/j.apcatb.2005.11.013.

Pozzo, R. L., M. A. Baltanás, and A. E. Cassano. 1997. "Supported Titanium Oxide as Photocatalyst in Water Decontamination: State of the Art." *Catalysis Today* 39, no. 3: 219–231. https://doi.org/10.1016/S0920-5861(97)00103-X.

Pugnet, V., S. Maury, V. Coupard, et al. 2010. "Stability, Activity, and Selectivity Study of a Zinc Aluminate Heterogeneous Catalyst for the Transesterification of Vegetable Oil in Batch Reactor." *Applied Catalysis A: General* 374, no. 1–2: 71–78. https://doi.org/10.1016/j.apcata.2009.11.028.

Quantachrome Instruments. 2009. *Autosorb iQ and ASiQwin: Gas Sorption System Operating Manual* (Model 7, ASiQwin Version 5.2; Part No. 05098-5.2 Rev B). Quantachrome Instruments.

Radhakrishnan, V. R., M. Ramasamy, H. Zabiri, et al. 2007. "A Kinetic Study of the Esterification of Free Fatty Acids (FFA) in Sunflower Oil." *Fuel* 86, no. 15: 2383–2388. https://doi.org/10.1016/j.fuel.2007.02.002.

Raj, K., and B. Viswanathan. 2009. "Effect of Surface Area, Pore Volume, and Particle Size of P25 Titania on the Phase Transformation of Anatase to Rutile." *Indian Journal of Chemistry—Section A* 48: 1378–1382.

Rajeshwar, K., M. E. Osugi, W. Chanmanee, et al. 2008. "Heterogeneous Photocatalytic Treatment of Organic Dyes in Air and Aqueous Media." *Journal of Photochemistry and Photobiology C: Photochemistry Reviews* 9, no. 4: 171–192. https://doi.org/10.1016/j.jphotochemrev.2008.09.001.

Salvadó-Estivill, I., A. Brucato, and G. L. Puma. 2007. "Two-Dimensional Modeling of a Flat-Plate Photocatalyticreactor for Oxidation of Indoor Air Pollutants." *Industrial and Engineering Chemistry Research* 46: 7489–7496. https://doi.org/10.1021/ie070391r.

Semwal, S., A. K. Arora, R. P. Badoni, and D. K. Tuli. 2011. "Biodiesel Production Using Heterogeneous Catalysts." *Bioresource Technology* 102: 2151–2161. https://doi.org/10.1016/j.biortech.2010.10.080.

Severson, K., M. Martín, and I. E. Grossmann. 2013. "Optimal Integration for Biodiesel Production Using Bioethanol." *AICHE Journal* 59: 834–844. https://doi.org/10.1002/aic.13865.

Shahidi, F. 2005. *Bailey's Industrial Oil and Fat Products*. 6th ed. Wiley.

Sharma, Y. C., and B. Singh. 2009. "Development of Biodiesel: Current Scenario." *Renewable and Sustainable Energy Reviews* 13, no. 6–7: 1646–1651. https://doi.org/10.1016/j.rser.2008.08.009.

Shobhana-Gnanaserkhar, N. Asikin-Mijan, G. AbdulKareem-Alsultan, Sivasangar-Seenivasagam, S. M. Izham, and Y. H. Taufiq-Yap. 2020. "Biodiesel Production via Simultaneous Esterification and Transesterification of Chicken Fat Oil by Mesoporous Sulfated Ce Supported Activated Carbon." *Biomass Bioenergy* 141: 105714.

Silva, C., A. Teixeira, S. Ferreira, and J. Santos. 2015. "Thermodynamic Analysis of Biodiesel Production by Transesterification Reaction." *Fuel Processing Technology* 138: 136–142. https://doi.org/10.1016/j.fuproc.2015.05.012.

Smith, R. M., and A. E. Martell. 2004. *Critical Stability Constants*. Vol. 6. Springer.

Sun, S., W. Wang, L. Zhang, M. Shang, and L. Jiang. 2009. "Ag_3PO_4 Photocatalyst for Visible-Light-Driven Water Oxidation." *Chemical Communications* 2009, no. 22: 3453–3455. https://doi.org/10.1039/B820299B.

Tauc, J., R. Grigorovici, and A. Vancu. 1966. "Optical Properties and Electronic Structure of Amorphous Germanium." *Physica Status Solidi* 15, no. 2: 627–637. https://doi.org/10.1002/pssb.19660150224.

Thanh, L. T., K. Okitsu, L. V. Boi, and Y. Maeda. 2012. "Catalytic Technologies for Biodiesel Fuel Production and Utilization of Glycerol: A Review." *Catalysts* 2, no. 1: 191–222. https://doi.org/10.3390/catal2010191.

Thanh, L. T., K. Okitsu, Y. Sadanaga, N. Takenaka, Y. Maeda, and H. Bandow. 2013. "A New Co-Solvent Method for the Green Production of Biodiesel Fuel – Optimization and Practical Application." *Fuel* 103: 742–748. https://doi.org/10.1016/j.fuel.2012.09.029.

Tomiya, I., Y. Wu, and K. Hyodo. 2024. "Ring-Opening Amino Esterification of Cyclic Ketones to Access Distal Amino Acid Derivatives." *Advanced Synthesis and Catalysis* 366: 1606–1614. https://doi.org/10.1002/adsc.202301421.

Van Gerven, T., G. Mul, J. Moulijn, and A. Stankiewicz. 2007. "A Review of Intensification of Photocatalytic Processes." *Chemical Engineering and Processing: Process Intensification* 46: 781–789. https://doi.org/10.1016/j.cep.2007.05.012.

Vicente, G., M. Martínez, and J. Aracil. 2004. "Integrated Biodiesel Production: A Comparison of Different Homogeneous Catalysts Systems." *Bioresource Technology* 92, no. 3: 297–305. https://doi.org/10.1016/j.biortech.2003.08.014.

Voegele, E. 2020. "NBB: Biodiesel Can Help Meet USDA's AIA Goals." *Biodiesel Magazine*. https://biodieselmagazine.com/articles/2517256/nbb-biodiesel-can-help-meet-usdaundefineds-aia-goals.

Welter, R. A., Jr., M. de Souza, M. Lopes, O. Taranto, and H. Santana. 2022. "Are Microreactors the Future of Biodiesel Synthesis?" In *The Future of Biodiesel*, vol. 1, 1st ed., 47–82. Nova Science Publishers Inc.

Welter, R. A., H. Santana, L. G. de la Torre, M. Robertson, O. P. Taranto, and M. Oelgemöller. 2022. "Methyl Oleate Synthesis by TiO_2 Photocatalytic Esterification of Oleic Acid: Optimisation by Response Surface Quadratic Methodology, Reaction Kinetics and Thermodynamics." *ChemPhotoChem* 6, no. 7: e202200007. https://doi.org/10.1002/cptc.202200007.

Welter, R. A., H. Santana, J. Wau, O. P. Taranto, and M. Oelgemöller. 2026. "TiO_2 Photocatalysed Biodiesel Production Through Simultaneous Esterification and Transesterification of Waste Cooking Oil." *Biomass Futures* 1: 100032. https://doi.org/10.1016/j.bmf.2026.100032.

Welter, R. A., H. S. Santana, L. Gaziola de la Torre, M. C. Barnes, O. P. Taranto, and M. Oelgemöller. 2023. "Biodiesel Production by Heterogeneous Catalysis and Eco-Friendly Routes." *ChemBioEng Reviews* 10, no. 2: 86–111. https://doi.org/10.1002/CBEN.202200062.

Wen, Z., X. Yu, S. T. Tu, J. Yan, and E. Dahlquist. 2009. "Biodiesel Production From Waste Cooking Oil Catalyzed by TiO_2–MgO Mixed Oxides." *Bioresource Technology* 100, no. 23: 6033–6040. https://doi.org/10.1016/j.biortech.2009.06.049.

Wnorowska, U., K. Niemirowicz, and R. Bucki. 2021. "Antimicrobial and Biodegradation Properties of Biodiesel Fuels." *Fuel* 285: 119080. https://doi.org/10.1016/j.fuel.2020.119080.

Yan, S., C. Dimaggio, S. Mohan, M. Kim, S. O. Salley, and K. Y. S. Ng. 2010. "Advancements in Heterogeneous Catalysis for Biodiesel Synthesis." *Topics in Catalysis* 53, no. 11–12: 721–736. https://doi.org/10.1007/S11244-010-9460-5.

Yan, S., S. O. Salley, and K. Y. S. Ng. 2009. "Simultaneous Transesterification and Esterification of Unrefined or Waste Oils Over

17571707, 2026, 6, Downloaded from https://onlinelibrary.wiley.com/doi/10.1111/gcbb.70113 by James Cook University, Wiley Online Library on [10/11/2026]. See the Terms and Conditions (https://onlinelibrary.wiley.com/terms-and-conditions) on Wiley Online Library for rules of use; OA articles are governed by the applicable Creative Commons License

ZnO-La_2O_3 Catalysts." *Applied Catalysis A: General* 353: 203–212. https://doi.org/10.1016/j.apcata.2008.10.053.

Yang, X., Y. Zhang, Z. Liu, and J. Wang. 2024. "Visible-Light-Driven Photocatalytic Transesterification for Biodiesel Production Using Modified TiO_2 Catalysts." *Fuel* 356: 129645. https://doi.org/10.1016/j.fuel.2023.129645.

Yao, Y., G. Li, S. Ciston, R. M. Lueptow, and K. A. Gray. 2008. "Photoreactive TiO_2 Nanotube Arrays for the Degradation of Organic Contaminants." *Environmental Science & Technology* 42, no. 13: 4952–4957. https://doi.org/10.1021/es800602f.

Yue, L., Q. Zhao, H. Li, and Y. Chen. 2024. "Microwave-Assisted Heterogeneous Catalytic Transesterification for Biodiesel Production: Process Intensification and Kinetic Analysis." *Bioresource Technology* 389: 129857. https://doi.org/10.1016/j.biortech.2023.129857.

Yurdakal, S., G. Palmisano, V. Loddo, V. Augugliaro, and L. Palmisano. 2008. "Nanostructured Rutile TiO_2 for Selective Photocatalytic Oxidation of Aromatic Alcohols to Aldehydes in Water." *Journal of the American Chemical Society* 130: 1568–1569.

Zanjani, N. G., A. K. Pirzaman, and E. Yazdanian. 2020. "Biodiesel Production in the Presence of Heterogeneous Catalyst of Alumina: Study of Kinetics and Thermodynamics." *International Journal of Chemical Kinetics* 52: 472–484. https://doi.org/10.1002/kin.21363.

Zhao, F., D. Cambié, J. Janse, et al. 2017. "Scale-Up of a Luminescent Solar Concentrator-Based Photomicroreactor via Numbering-Up." *ACS Sustainable Chemistry & Engineering* 6: 422–429.

Zhou, H., H. Lu, and B. Liang. 2006. "Solubility of Multicomponent Systems in the Biodiesel Production by Transesterification of *Jatropha curcas* l. Oil With Methanol." *Journal of Chemical & Engineering Data* 51: 1130–1135. https://doi.org/10.1021/je0600294.

Supporting Information

Additional supporting information can be found online in the Supporting Information section. **Data S1:** gcbb70113-sup-0001-supinfo1.pdf. **Table S9:** gcbb70113-sup-0002-Table-S9.xlsx.

17571707, 2026, 6, Downloaded from https://onlinelibrary.wiley.com/doi/10.1111/gcbb.70113 by James Cook University, Wiley Online Library on [10/11/2026]. See the Terms and Conditions (https://onlinelibrary.wiley.com/terms-and-conditions) on Wiley Online Library for rules of use; OA articles are governed by the applicable Creative Commons License